Spring 5-2024

Modeling of NK Cells in Pediatric Patients With Unusually Severe or Recurrent HSV Using High-Dimensional Flow Cytometry

Yunran Feng
Washington University – McKelvey School of Engineering

WASHINGTON UNIVERSITY IN ST. LOUIS

McKelvey School of Engineering
Department of Biomedical Engineering

Thesis Examination Committee:
Jai Rudra, Chair
Katherine Schreiber
Michael Vahey

Modeling of NK Cells in Pediatric Patients With Unusually Severe or Recurrent HSV Using High-Dimensional Flow Cytometry

by

Yunran Feng

A thesis presented to
the McKelvey School of Engineering
of Washington University in
partial fulfillment of the
requirements for the degree
of Master of Science

May 2024
St. Louis, Missouri

Table of Contents

List of Figures

List of Tables

List of Abbreviations

FACS	Fluorescence-activated Cell Sorting
FCS	Fetal calf serum
FNKD	Functional NK cell deficiency
HSV	Herpes simplex virus
LRS	Leukoreduction system
NK	Natural killer
NKG2D	Natural killer group 2, member D (KLRK1, Killer Cell Lectin-Like Receptor K1)
PBMC	Peripheral blood mononuclear cells
PLCG2	Phospholipase C-γ 2

Acknowledgments

I would like to express my sincere gratitude to my supervisor, Dr. French, for his guidance and support throughout my research journey. His expertise and insight have been instrumental in my academic journey. I am also grateful to Jeanette, our lab manager, not only for her assistance in the lab, but also for encouraging me when I was discouraged about negative results.

I want to express my gratitude to the pediatric department and BME department for academic and financial support. Their backing has been crucial in the success of this work.

I want to express my appreciation to the patients and their families who donated blood samples over the past ten years, making this research possible. I am also deeply thankful to the Center for Pediatric Immunology at Washington University and St. Louis Children's Hospital for providing us with precious age matched control samples. I extend my thanks to the blood bank for providing the Leukoreduction System Chambers, which are essential resources for our study.

I want to express my appreciation to all the professors and teachers who have taught me these years. The knowledge and insights I gained from them have been foundational to my growth and success in my field.

Lastly, I must also express my deepest thanks to my family and friends for their constant support and encouragement. They have been my steadfast source of motivation and strength.

Yunran Feng

Washington University in St. Louis

May 2024

ABSTRACT OF THE THESIS

Modeling of NK Cells in Pediatric Patients With Unusually Severe or Recurrent HSV Using High-Dimensional Flow Cytometry

by

Yunran Feng

Master of Science in Biomedical Engineering

Washington University in St. Louis, 2024

Professor Jai Rudra, Chair

HSV infection is broadly spread all over the world with some patients having severe and/or recurrent HSV infections. Our lab studies human Natural Killer (NK) cells, which are important in innate immune responses to viral infections and tumors. A publication in 2013 by Ornstein et al from our lab studied HSV+ pediatric patients and found some associations between severe infection and defects in NK cytolytic function. *PLCG2* haploinsufficient variants found in 2 HSV patients causing PLCγ2 hypophosphorylation, and loss of cytolytic function in NK cells is a novel finding recently published by Alinger et al from our lab in 2023. Prior to that study, *PLCG2* gain of function variants in B cells had been well studied but loss of function had not been reported in the context of human NK cells in patients with recurrent HSV infection. This project is a continuing study to determine whether PLCγ2 hypophosphorylation in NK cells is shared by many HSV+ patients. Our focus is to look for any differences in PBMC immune profiles and NK profiles in the patients and perform cytotoxic assay and PLCγ2 phosphorylation status of NK cells using flow cytometry.

This project required learning spectral flow and processing the results to analyze the high-dimensional data. We aimed to analyze an extensive immune profiling panel containing 19 colors for patients' PBMCs using spectral flow cytometry. The Cytek Aurora is a state-of-the-art

cytometer which has 5 lasers and 64 channels. An additional NK panel will delineate the maturation and activation state of NK cells. Spectral flow cytometry is a powerful immunoprofiling tool detecting up to 40 markers on a single blood sample, which enables us to collect large datasets using a minimal number of cells.

All patient samples in this thesis are collected from children who have severe or unusually recurrent herpesvirus (HSV) infections. We analyzed 3 sets of patients each compared to an age- and sex- matched control. Unfortunately, in two of three sets, the age-matched controls had unusually low cytolytic activity, making it difficult to draw any conclusions about the two sets of corresponding patient profiles. In the other set where the control cells were normal range for cytolytic ability, we found one pediatric HSV patient with a significant defect in their ability to lyse K562 targets. This young female patient with the cytolytic defect surprisingly had PLCγ2 hyper-phosphorylation in NK cells instead of hypophosphorylation as expected.

She also has a normal immune cell profile, but a more terminally mature NK profile ($CD57^+$) compared to the healthy control. This finding correlates to Alinger's characterization of a female pediatric HSV+ patient with PLCγ2 defects in their work. In general, NK-cell immunodeficiency may be related to abnormal PLCγ2 functions and an increased number of $CD57^+$ NK cells.

Chapter 1: Introduction

Herpesviruses Infection

Herpes simplex virus 1 (HSV-1), HSV-2, and cytomegalovirus (CMV) are the most common types of herpesviruses, and their infections are very common all over the world. The infection of HSV-1 is usually acquired and spread during childhood and adolescence. The pooled mean HSV-1 seroprevalence was 57.2% in healthy children and 84.5% in healthy adults in 2018[1]. HSV-1 usually infects via the oral or genital mucosa and the symptoms may present as cold sores or fever blisters in or around the mouth or genitals.

HSV infection symptoms may be mild or even undetected. According to a paper published in 2014, 52% of women involved in the Herpevac (a Herpes Simplex Vaccine) trial were unaware of any HSV infection but had positive HSV-1 status.[2] Most healthy individuals with HSV will experience mild symptoms and do not need medical treatment. However, some patients who are immunocompromised will experience severe and/or frequent HSV infections and need antiviral treatment. In a previous work of our lab, Ornstein and colleagues broadly analyzed the phenotype and function of natural killer (NK) cells in pediatric patients with severe and/or recurrent HSV infections and compared them to healthy age-matched control populations. Interestingly, five out of fifteen patients showed a decrease in NK cell cytotoxicity. Two of those five had possible explanations for why their NK cells were functionally defective. One of them had NK cell degranulation problems and low CD11b expression, which influences NK cell adhesion and cytolytic activity. Another patient had significantly higher expression of ILT-2 (Ig-like transcript 2), which is an inhibitory receptor. ILT-2 problems are reported to lead to problems in NK cytotoxic activity.[3],[4] The explanations for NK functional defects in the other three patients were

not clear at that time. Also, they found no global differences in NK degranulation measured by surface CD107a expression or NK interferon-γ production by intracellular staining after coculture with K562 target cells for 8 hours.[3] Alinger also studied the relationship between severe and/or recurrent HSV infections and NK cell dysfunction and more details will be shown in a later section.

NK cell function

Human NK cells, defined by CD56 positive CD3 negative expression in human peripheral blood mononuclear cells (PBMC), are important innate lymphocytes in both antiviral and antitumor processes.

In healthy people, the NK cell range in PBMC is 5%-20%. The function of NK cells changes during their development and is marked by a change in surface proteins. At early stages, both NKG2D and CD56 expression are negative, and NK cells are not functioning in immune responses. The majority of NK cells in PBMC are divided into two groups, CD56 bright or dim. $CD56^{bri}$ NK cells play the most important role in cytokine production. As NK cells mature, CD56 expression becomes dim and CD16 starts to express. This $CD56^{dim}CD16^{+}$ NK phenotype is more mature, and this population is responsible for NK cell cytotoxicity.[5]

NK cells kill aberrant cells by secreting perforin and granzyme molecules. Unlike cytotoxic T cells, NK cells are naturally cytotoxic and do not require a prior antigen-presenting process. They recognize virus-infected cells through many different activation receptors. For example, NK cells can recognize herpesvirus-infected cells through non-HLA-I-specific activating receptors and co-receptors (e.g., NKG2D and 2B4), which will directly recognize cellular ligands on target cells. The NKG2D receptor is made up of one NKG2D homodimer and two DAP10 homodimers. Once NKG2D binds with their ligands, the two DAP10 associated with NKG2D will be phosphorylated.

The phosphorylated DAP10 will recruit PI3K or Grb2 and then activate the downstream signaling pathways (Figure 1.1 A).[6] Another mechanism in NK recognition of herpesvirus-infected cells is antibody-dependent cellular cytotoxicity (ADCC) mediated by Fcγ receptors (FcγR), especially FcγRIIIA, i.e., CD16.[6,7] CD16 binds to the Fc portion of IgG on some aberrant cells. Once the crosslinking signal appears, the tyrosine residues in immunoreceptor tyrosine-based activation motifs (ITAMs) on CD16 are phosphorylated, and the phosphorylated ITAMs recruit the spleen tyrosine kinase (Syk) and activate the downstream signaling pathways. (Figure 1.1 B)[8,9] Natural cytotoxicity receptors (NCRs) like NKp44 and NKp46 can also recognize their ligands and activate NK cells through ITAMs.[6,10]

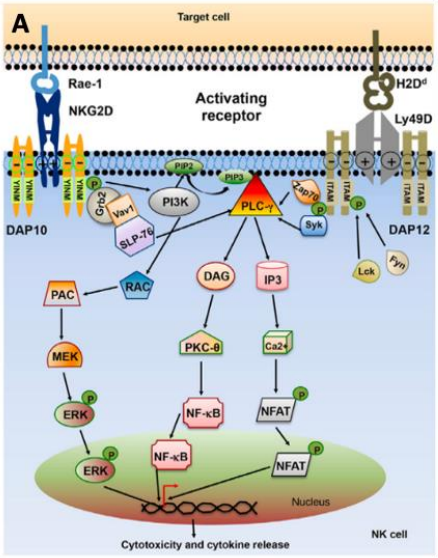

Front. Immunol. **2017**, *8*, 1124.

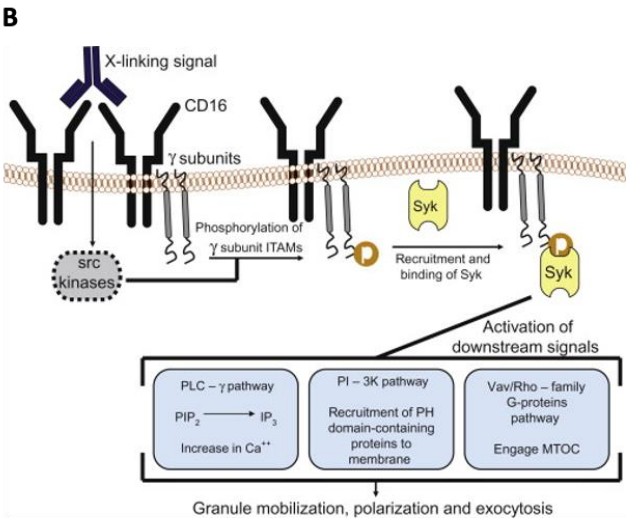

Immunol. Cell Biol. **2014**, *92* (3), 221–229

Figure 1.1 Schematic representation of NK cell activating receptor signaling. A. NKG2D pathway. Ligands binding to activating receptor NKG2D leads to phosphorylation of the tails present in the cytoplasm of the YINM motif of associated adapter protein DAP10. The phosphorylated YINM motif recruits Grb2/ Vav1/SLP-76 complex which then recruits and activates PLCγ which activates downstream signaling pathways *(Front. Immunol.* **2017**, *8*, 1124.) B. CD16 pathway. After CD16 cross-linking, src kinases are activated, and then the ITAMs on the γ subunits **are** phosphorylated, which then recruit Syk and activate the PLC-γ pathway, and other pathways. *(Immunol. Cell Biol.* **2014**, *92* (3), 221–229)

NK cell deficiency (NKD)

The NK cell population in human PBMC ranges between 5%-20%. NK cell deficiency is a subset of primary immunodeficiencies although very small, and thus challenging to diagnose and treat. Those patients with absent NK cells are diagnosed with classical NKD (CNKD). Functional NKD (FNKD) may be diagnosed when NK cell numbers are within the normal range or slightly decreased, but NK cells' cytotoxic activities are significantly decreased. Low expression of CD16 was found to be related to one subtype of FNKD, but the other subtypes were not yet studied.[11] In Ornstein's study, three patients had low cytolytic activity in NK cells for an unknown reason.

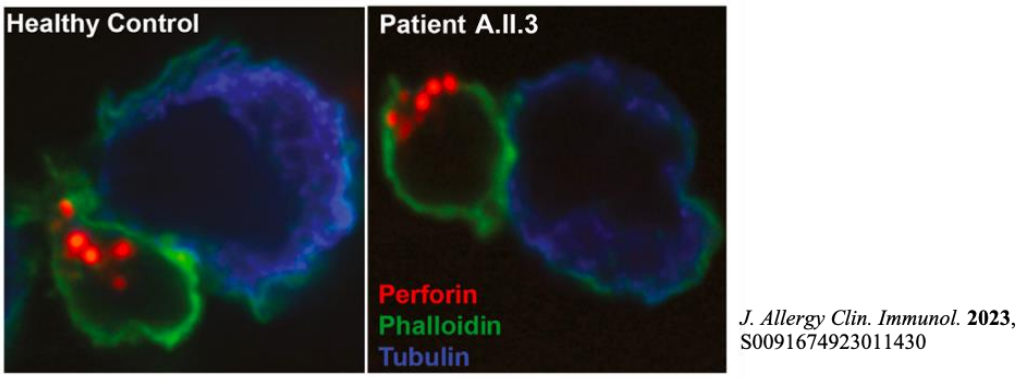

Figure 1.2 Representative immunofluorescence confocal microscopy image. The large cell represents the K562 cell, and the small cell is the NK cell. *J. Allergy Clin. Immunol.* **2023**, S0091674923011430

In another study by our lab, Alinger and colleagues found that two distinct *PLCG2* variants (G595R and L183F) are related to FNKD. They studied two pediatric HSV patients with severe and/or recurrent infections from two unrelated nonconsanguineous families, and in a G595R *PLCG2* variant patient, they found a defect in the ability of their NK cells to lyse targets, despite normal degranulation measured by CD107a. They used confocal microscopy to look at the degranulation process in this patient and compared it to a healthy control (Figure 1.2). PBMCs and K562 target cells were cocultured for 45 minutes and then fixed, permeabilized, and stained. The

granules from healthy NK control cells are released into the immunological synapse with the target, while in the G595R *PLCG2* patient, granules are not moving toward the synapse, which explains the defect in cytolytic function.[12]

PLCγ2 mechanisms and functions

PLCG2 encodes phospholipase C-γ2 (PLCγ2), which is one common downstream signal of the aforementioned NK cell activation mechanisms. PLCγ2 is necessary in B cells and NK cells. Once NK cells are activated, PLCγ2 in NK cells is recruited and phosphorylated by LAT (linker for activation of T cells). The phosphorylated PLCγ2 (pPLCγ2) will then cleave phosphatidylinositol-4,5-bisphosphate (PIP_2) to generate inositol-1,4,5-trisphosphate (IP_3) and diacylglycerol (DAG)[13]. The IP_3 activates the inositol trisphosphate receptor (IP3R) and then causes an increase in cytosolic calcium levels, which is important for cytotoxic granule release into the synapses between NK cells and the aberrant cells. [14,15]

As aforementioned, Alinger et al studied one HSV patient with the G595R *PLCG2* variant and her parent with the same mutation. They measured PLCγ2 phosphorylation in $CD56^{dim}$ NK cells after CD16 crosslinking and found the patient and her mother had significantly lower phosphorylation compared to the healthy control. They also measured calcium flux in $CD56^{dim}$ NK cells and found that it was lower in this patient than in the age-matched healthy controls. They used confocal microscopy and showed the G595R *PLCG2* variant NK cells produced granules but there was a problem in granule migration toward the synapse between the effector and target cell.

Alinger's study showed a novel finding that the loss-of-function mutations due to PLCG2 haploinsufficiency caused herpesvirus susceptibility and FNKD in humans. Previously the most studied *PLCG2*-related diseases were PLAID (*PLCG2*-associated antibody deficiency and

immune dysregulation) and APLAID (Autoinflammatory *PLCG2*-associated antibody deficiency and immune dysregulation), in which the gain-of-function *PLCG2* variants in B cells play the major role. The dysregulation of B cells and/or mast cells, not NK cells, causes those predominant clinical phenotypes. [16,17,18] In a more recent study done by Michael Ombrello's group, *PLCG2* variants were found related to phenotypes other than PLAID. They studied 76 patients with known *PLCG2* variants and identified 60 distinct protein-altering variants of *PLCG2*. Most of these patients have recurrent or atypical infections but do not have cold urticaria, which is the hallmark of PLAID. They studied the function of those patient *PLCG2* variants using a transfected chicken B cells model and found that 42 of these variants had an impact on calcium flux and/or ERK phosphorylation after stimulation. Twenty-nine of the 42 variants cause reduced calcium flux and/or reduced ERK phosphorylation, while 13 variants cause increased calcium flux and hyperphosphorylation of ERK in B cells. Four multigenerational families have recurrent bacterial and/or viral infections and their *PLCG2* variants are T292M, N1097del, L170F, and E565D. Therefore, they pooled them together to form a smaller cohort and studied NK cell function. Low NK cell numbers were found in three families. Decreased NK cell cytotoxicity was found in two families. Two additional singleton probands (L183F and H193Q) had similar recurrent invasive viral infections and NK-cell defects. The L183F *PLCG2* variant had also been reported and investigated in Alinger's study. This mutant displayed low NK cell cytotoxicity, low NK cell calcium flux in response to stimulation through NKG2D and 2B4, and low PLCγ2 phosphorylation in response to CD16 but normal NK cell numbers.[19]

Ombrello's group was curious about whether NK-cell functional impairment is more pronounced and widespread than B-cell defect. The correlation between their interest and what Alinger found regarding two *PLCG2*-variants related to human NK cell deficiency makes it important and

meaningful to continue expanding the sample size and continue to conduct PLCγ2-related research in the context of NK cell function.

Previous work of our lab and current research interests

Ornstein et al reported that one-third of severe and/or recurrent HSV patients in his study panel of 15 members had NK cell cytolytic defects, however, he was not able to determine a genetic diagnosis responsible for this NK loss of function phenotype. Years later, Alinger was inspired to further investigate whether PLCG2 variants found in 2 new pediatric patients with recurrent HSV infections may play a role in their B cell and NK cell functions.

Using whole exome sequencing, Alinger found some medium to high-impact variants and compared them across those two patients and their parents. One affected gene that the patients and one parent had in common was *PLCG2*. One patient had an L183F *PLCG2* variant and the other patient and her mother shared the same G595R *PLCG2* variant. A 3-D molecular structure of the G595R variant was simulated using PyMOL. The G595R mutation was found in a protein-protein interaction loop in PLCγ2 which potentially compromises the LAT phosphotyrosine binding site and therefore decreases the phosphorylation level of PLCγ2.[12]

They performed functional assays including NK cell cytotoxicity, degranulation, and calcium flux for both NK cells and B cells, and most of the differences were found in the NK cells. In healthy controls, NK cell PLCγ2 gets phosphorylated significantly within a 5-minute range once they are stimulated through CD16 crosslinking, however, NK cells of the two patients with *PLCG2* variants show lower PLCγ2 phosphorylation in response to CD16 crosslinking. This data correlates with lower calcium flux in response to 2B4 and NKG2D crosslinking seen in patient NK cells compared to that of healthy controls. The B cell function in these patients, however, was the same as in

healthy controls. Activated NK cell interferon-γ (IFN-γ) secretion levels in both families were normal. They used confocal microscopy to further examine degranulation in the G595R patient and found the cytotoxic granules were released but did not migrate to the synapse, which explains normal degranulation detected by CD107a but low cytolytic activity against K562 targets.

They designed a large immunoprofiling panel and found the total B cell level of G595R patient and her affected mother is lower than normal, however, the proportion of naïve B cells and class-switched B cells are about the same. The mononuclear myeloid cells are at a lower level. The NK cell populations and the ratio of $CD56^{dim}$ and $CD56^{bri}$ in these patients are within a healthy range. They also found the NK cells in the G595R patient were in a more mature state but lost the $NKG2C^{+}$ population compared to the healthy control.[12]

As aforementioned, Ornstein and colleagues analyzed the phenotype and function of NK cells in HSV+ pediatric patients and compared them to the controls. They found one-third of patients have NK cell cytotoxicity defects. Low CD11b expression level in one patient and higher expression of ILT-2 in another patient may be the cause of their low cytotoxic activity.[3] However, the mechanisms of the NK functional defects in the other three patients were not clear at that time. They also did not find global differences in IFN-γ production in the HSV+ patients compared to healthy controls.

Due to previous technological limitations of flow cytometers and limited fluorochrome availability, Ornstein et al. did not have an opportunity to analyze the complete profile of blood immune cell types in their study. They were, however, able to study a panel of some NK-specific surface markers and secreting molecules by setting up multiple flow runs using a BD FACSCalibur, which required many patient cells due to the limited fluorochromes at that time.

They found some differences between patients and healthy controls. The NKp44 expression was slightly increased, which indicates that the HSV+ patients' NK cells are activated in the challenge of viruses. The expression level of NKG2D, which is a stimulatory receptor, and Granzyme A and perforin, which are cytolytic molecules, were slightly decreased. However, this finding was not enough to explain why those three patients had NK cell-killing defects.[3]

In Alinger's study, cytometry by time of flight (CyTOF) was used to collect complete profiles of blood immune cell types for the *PLCG2* variant patient. CyTOF was the most advanced technology at that time. It uses heavy metal antigen conjugates and uses the mass difference to separate those markers from each other, which makes it possible to include more markers on cells in the same test. Unlike the limited capabilities of flow cytometry at that time, CyTOF offered the opportunity to study many features in a small number of cells. This technique is still available, however very costly. In our lab, it has now been replaced by Spectral Flow cytometry in parallel with an increase in fluorochrome expansion and availability.

Spectral Flow, which is a high-dimensional flow cytometry developed over the last decade, enables us to look at a much larger panel of markers on one cell than previously allowed. Therefore, we can collect a complete blood immune profile with 19 markers to study PBMC profiles of our patient samples using fewer cells and in less time.

The study of human NK cells is always limited by the scarcity of patient samples. In Alinger's study, he tried to expand the patient cells by culturing the NK cells on an irradiated feeder layer of K562mbIL15-41BBL cells and IL-2 before analysis. The expanded cells showed restored cytotoxicity and calcium flux levels. These findings make the patient samples more precious since we cannot use this approach to expand NK cells for functional studies.

In general, Ornstein's and Alinger's findings inspired me greatly. These findings indicated that a proportion of pediatric patients with severe and/or recurrent HSV infections might have FNKD due to *PLCG2* variants. Our goal is to investigate whether there is a relationship between PLCγ2 and NK cell function in a current pool of HSV-infected pediatric patients. The impaired PLCγ2 phosphorylation may characterize a subtype of NKD. Studying this could help categorize rare HSV patients who do not exhibit typical immunodeficiencies.

The same panels of patients from those examined in Ornstein's paper and Alinger's paper are no longer available for us to study, so we will focus on a new group of HSV+ pediatric patients collected over 10 years. This panel of HSV+ pediatric patients experiencing severe symptoms or recurrent infections is previously unstudied. Two extensive spectral flow panels consisting of a 19-color PBMC immune profiling panel and the other, an 11-color panel focusing on NK maturation state and activation markers. In addition, NK cell cytotoxicity assays will the first tier of study. Those patients with NK functional defects will be studied further, looking at PLCγ2 expression and phosphorylation profiles in response to CD16 crosslinking in their NK cells. Of those who show impaired PLCγ2 phosphorylation, we planned to repeat the NK cytolytic assays, study NK cell degranulation, and also conduct NK calcium flux experiments in response to NKG2D and 2B4 crosslinking as patient sample availability allows. Because the patient samples are very precious, we first optimized all protocols on human PBMCs from apheresis unit leukoreduction system (LRS) chambers following routine platelet donations. The details of all these assays will be shown in the Methods section (Chapter II), and the experiment with LRS including the optimization of methods and troubleshooting will be shown in Chapter IV.

Chapter 2: Materials and Methods

2.1 Cell Culture

Unless specifically mentioned, all the cells are cultured in cR10 (complete RPMI with 10% Fetal Calf serum) in a Heracell™ VIOS 160i CO2 Incubator (Thermo) at 37°C with 5% CO_2. Where indicated, cells are washed by either cR10, wash buffer, FACS (Fluorescence-activated Cell Sorting) buffer, permeabilization buffer, or PBS (Phosphate-buffered saline). The recipes for these buffers and the information about the reagents used to prepare the buffers are shown in detail in Appendix Table. S1

2.2 Sample collection and preparation

2.2.1 Patient and sample collection

Samples from six pediatric patients with a recurrent HSV infection history in addition to age-matched controls (AMC) are obtained using written informed donor consent through St. Louis Children's Hospital. All are used with the approval of the Washington University School of Medicine Institutional Review Board. The healthy age-matched controls included in the study are either collected and processed by previous members of our lab or requested from the Center for Pediatric Immunology at Washington University and St. Louis Children's Hospital.

2.2.2 Isolating PBMC from blood donation and leukoreduction system (LRS) chamber

The donor blood arrives at the lab in several 15 ml heparinized blood collection tubes (BD Vacutainer). The tubes are placed on a rocker for 1 hour at room temperature and then transferred into a 50 ml conical tube (Corning). Equal volume of PBS is added to the tube to a maximum of 35 ml volume. The tube is inverted several times to mix the PBS with blood. The blood mixture is underlaid by 5 ml of Ficoll (GE Healthcare) at room temperature. After that, the tube is centrifuged

at 2000 rpm, ROOM TEMPERATURE, 20 minutes with no brake on using a Beckman Allegra 6R Refrigerated Benchtop Centrifuge (Beckman Coulter). The plasma is removed and then the cotton-like layer, which contains the white blood cells, is transferred to a 50 ml conical tube with 10 ml PBS. The volume is brought up to 30 ml with PBS and then to 50 ml with cR10. After 10 minutes of centrifuge at 1500 rpm, with brake, the supernatant is removed, and the cells are resuspended in 500 μl cold cR10. Cells are diluted to the intended concentration with cR10, and frozen back at various concentrations by mixing with freezing buffer (20% Dimethyl sulfoxide in FCS) 1:1 and transferred to Nalgene™ General Long-Term Storage Cryogenic Tubes (Thermo Scientific). Samples are placed in a Nalgene® Cryo 1°C 'Mr. Frosty' Freezing Container (Thermo Scientific) at -80°C and transferred to liquid nitrogen storage two days later.

The LRS chambers are provided by the BJC blood bank. Methods to process blood cells from the LRS chamber are the same as those for patient blood samples except for the first few steps before adding Ficoll. A 60 ml syringe (BD) filled with PBS is used to flush the blood cells from the LRS chamber into 50 ml conical tubes (15 ml per tube). PBS is added to all the tubes to meet the 35 ml max total volume. After that, tubes are capped and inverted several times and the remaining steps from the Ficoll underlay to cryopreservation are the same as for donor PBMCs.

2.2.3 Thawing PBMC

The vial of frozen PBMC is quickly thawed in a 37°C water bath and transferred to a round bottom 15 ml Falcon 2046 tube on ice. A total of 1.2 ml cold FCS is slowly added to the tube dropwise over 3-5 minutes. The cells rest for 2 more minutes on ice and are centrifuged at 1300 rpm, 4°C, for 5 minutes. After removing the supernatant, cells are gently resuspended in a volume to make the concentration close to 1×10^7 cells/ml with warm cR10 and transferred to a 37°C water bath to rest for one hour.

2.3 Spectral flow cytometry

Traditional flow cytometry uses photodetectors for each fluorochrome, and the overall number of fluorochrome is limited. Spectral flow cytometry is a more advanced technique that uses an array of detectors that capture the entire emission spectrum (64 channels) of all fluorochromes used on a same sample. With this method, multiple characteristics of the same cell can be captured at one time, and we can do a more comprehensive cell analysis. The spectral flow cytometry is used to collect the total PBMC and NK panel profiles, in addition to PLCγ2 studies and cytolytic assays. The acquisition is performed using a 5-laser Cytek Aurora cytometer.

2.3.1 Cell panel preparation

The first step for collecting the immune cell subpopulation profile and NK cell activation and maturation state profile is staining 1.5×10^6 cells with viability dye. PBMCs are rested for an hour after thaw and then washed with 15 ml PBS (with 5% serum). 1.5×10^6 cells are stained with 1.5 μl LDB (Live/Dead Blue stain, Thermos Fisher Scientific) in 1.5 ml PBS for 30 minutes at room temperature. The cells are then washed with 15 ml warm cR10 and resuspended in 100 μl and divided into two microfuge tubes with 5×10^5 cells per tube for PBMC and NK panel staining.

2.3.2 Immune Cell Subpopulation Profile

A total of 19 fluorochromes (Table 2.1) are used for the immune cell subpopulation profiles for 5×10^5 PBMC. After LDB staining and washing, 18 fluorochrome-conjugated antibodies for surface staining are mixed together and added to PBMCs for 30 minutes at room temperature. The data is collected using a 5-laser Aurora (Cytek) and analyzed using FlowJo (BD). The first gate for cells is settled according to the forward scatter area (FSC-A) and side scatter area (SSC-A). Then single cells are selected by FSC-A and forward scatter height (FCS-H). Live PBMCs are

identified by Live/Dead Blue signal intensity in the singlet PBMC gate, and the live immune cells are further identified by CD45 positive signals. From there, B cells, NK cells, T cells, monocytes, and Dendritic cells (DC) populations are gated according to different surface markers. The gating strategy is shown in Appendix Figure S1.

Table 2.1 Antibodies used for PBMC Panel

Name	Clone	Vendor	Catalogue number
LIVE/DEAD Fixable Blue Dead Cell Stain Kit	N/A	Thermo Fisher Scientific	404-0259-42
Cytek® 25-color Immunoprofiling Assay cFlour® reagent Kit	N/A	CYTEK	R7-40002
cFluor V450 anti-Hu CD45RA	HI100	CYTEK	R7-20122
cFluor B532 Anti-Hu CD8	SK1	CYTEK	R7-20124
cFluor B548 Anti-Hu CD14	63D3	CYTEK	R7-20116
cFluor B690 Anti-Hu HLA-DR	L243	CYTEK	R7-20126
cFluor YG584 Anti-Hu CD4	SK3	CYTEK	R7-20042
cFluor BYG667 Anti-Hu IgD	IA6-2	CYTEK	R7-20138
cFluor BYG781 Anti-Hu CD11c	3.9	CYTEK	R7-20132
cFluor R659 Anti-Hu CD127	A019D5	CYTEK	R7-20078
cFluor R685 Anti-Hu CD19	HIB19	CYTEK	R7-20118
cFluor R720 Anti-Hu CD123	6H6	CYTEK	R7-20014
cFluor R780 Anti-Hu CD45	2D1	CYTEK	R7-20134
cFluor R840 Anti-Hu CD27	QA17A18	CYTEK	R7-20082
Brilliant Violet 510TM anti-human IgM	MHM-88	Biolegend	314521
Brilliant Violet 785TM anti-human CD279(PD-1)	EH12.2H7	Biolegend	329929
Brilliant Violet 570TM anti-human CD3	UCHT1	Biolegend	300435
Brilliant Violet 750TM anti-human CD56	5.1H11	Biolegend	362555
Anti-Hu CD25, eBioscience Brilliant VioletTM 421	BC96	Thermo Fisher Scientific	404-0259-42
PE/Dazzle594 anti-human CD16 Anti-Hu CD16	3G8	Biolegend	302053

2.3.3 NK Profile

Table 2.2 Antibodies used for NK Panel

Name	Clone	Vendor	Catalogue number
LIVE/DEAD Fixable Blue Dead Cell Stain Kit	N/A	Thermo Fisher Scientific	404-0259-42
PE mouse anti-human NKp44 CD336	p44-8.1	BD biosciences	558563
BUV737 Mouse Anti-Human CD314 (NKG2D)	1D11	BD biosciences	748426
BB700 Mouse Anti-Human NKG2A(CD159a)	131411	BD biosciences	747926
BUV563 Mouse Anti-Human CD11b	D12	BD biosciences	748589
NKG2C Antibody, anti-human, PE-Vio®770 REAfinity	REA205	Miltenyi Biotec	130-120-449
Pacific BlueTM anti-human CD57	HNK-1	Biolegend	359608
Brilliant Violet 605TM anti-human Ki-67	Ki-67	Biolegend	350522
APC/FireTM 759 anti human CD69	FN50	Biolegend	310946
BUV395 Mouse anti-human CD3	SK7	BD biosciences	564001
APC anti-human CD56 (NCAM)	5.1H11	Biolegend	362504

Similar to the immunoprofiling, 5×10^5 LDB-stained PBMCs are stained with all the surface markers (Table 2.2) at the same time after LDB staining for the NK panel. After collecting all the

data on a Cytek Aurora, FSC-A and SSC-A parameters are used to set the gate for all PBMCs. Live PBMCs are identified by Live/Dead Blue signals, and then single cells are selected by FSC-A and FSC-H. Lymphocytes are identified by forward and side scatter characteristics in the single cell gate and NK cells are identified by $CD56^{+}CD3^{-}$ in the lymphocyte gate. The expressions of NKG2D, NKG2C, CD69, etc. are analyzed by the signal intensity and shown by the percentage of positive staining based on an initial NK cell gate. For the maturation status, NK cells are identified by $NKG2D^{+}CD3^{-}$ in the lymphocyte gate. The signal intensity of CD56, together with CD57, is used to represent maturation.

2.3.4 Dimension Reduction and Visualization

Dimension reduction and visualization of the spectral flow data are done by t-Distributed Stochastic Neighbor Embedding (tSNE). The tSNE is performed using FlowJo opt-tSNE[20], with 1000 iterations, and the perplexity is set at 10. We used ANNOY and FFT interpolation for the embedding.[21]

2.4 NK cell cytotoxicity assays

Human K562 tumor cells (American Type Culture Collection [ATCC] CCL 243) are used as targets in this NK cytotoxicity assay. K562s are labeled with 0.25μM Cell Trace Violet (Invitrogen) one day before doing the killing experiment. PBMCs from patients and age-matched controls are thawed and rested for one hour at 37°C in cR10. PBMCs are labeled with APC-CD56 (Biolegend) and BUV395-CD3 (BD biosciences) to identify NK cells. The percentage of NK cells in total PBMCs is analyzed using a Cytek Aurora flow cytometer prior to assay setup to calculate and normalize NK cell numbers across samples. The PBMCs are plated in technical duplicates or triplicates with Cell Trace Violet labeled K562s into 96-well U-bottom plates at a calculated NK-K562 ratio of 3:1 and 1:1. Four wells contain only Cell Trace Violet labeled K562s. Three wells

are plated to assess spontaneous background analysis and one well (TX-100 lysed K562) will serve as the positive control to ensure 7AAD can stain all the lysed cells. 7-AAD master mix is made by mixing 7AAD (Biolegend) and cR10 at a ratio of 1:4. After the cells are incubated at 37°C, 5%CO_2, for 4 hours, 25 µl of the 7-AAD master mix is added to each well, and 5ul of TX-100 is added to the positive control well. A Cytek Aurora is used to collect 2500 Cell Trace Violet labeled K562 events for each sample and the target cell death is quantified by 7AAD signal intensity in the K562 gate.

Table 2.3 Antibodies used for cytotoxicity assay

Name	Clone	Vendor	Catalogue number
BUV395 Mouse anti-human CD3	SK7	BD biosciences	564001
APC anti-human CD56	5.1H11	Biolegend	362504
7AAD	N/A	Biolegend	420404
CellTrace Violet Cell Proliferation Kit	N/A	Thermo Fisher Scientific	C34557

2.5 PLCγ2 expression level and PLCγ2 phosphorylation

PBMCs from patients, age-matched controls, or LRS chambers are thawed and rested for an hour at 37°C water bath in cR10 and then Fc receptors are blocked with 8.3% pooled human serum for 15 minutes at room temperature before starting the assays to measure total PLCγ2 expression level and PLCγ2 phosphorylation level. Foxp3/Transcription Factor Staining Buffer Kit (TONBO biosciences) is used in both assays for fix and permeabilization steps. Total PLCγ2 expression assay is done in singlets and the phosphorylation experiments are performed in duplicate.

2.5.1 Expression of total intracellular PLCγ2

1×10^6 Fc-blocked PBMCs are fixed for 45 minutes and then washed with permeabilization buffer Cells are divided into two tubes. All are stained in the permeabilization buffer at 4 °C overnight using either 0.00625ng PLCγ2-PE conjugated antibody or 0.00625ng PE-tagged IgG_1isotype control (Biolegend). After overnight staining, to identify NK cells, the PBMCs are stained in permeabilization buffer with APC-CD56 and BUV395-CD3 for 30 minutes at room

temperature. The cells are washed once with permeabilization buffer and then once with FACS buffer before acquisition using Cytek Aurora. The results are presented in mean fluorescent intensity (MFI) of cells within the NK cells gate ($CD56^{+}CD3^{-}$).

2.5.2 Phosphorylation profile of PLCγ2

3×10^{6} Fc blocked PBMCs are stained with the 25 μg/ml Ultra-LEAF purified anti-human CD16 (Biolegend) as the primary antibody and then washed with cR10. Cells are aliquoted into six tubes for duplicates at 3 time points. Cells are prewarmed at 37°C for 15 minutes. 10 μg/ml purified goat anti-mouse IgG (Biolegend) is added to crosslink with the anti-CD16 antibody and incubated for 0, 1, and 5 minutes. Cells are fixed right after stimulation, incubated on ice for 45 minutes and then washed with perm buffer. Fc block is added again in the same concentration after perm buffer wash, 15 minutes before staining the phosphorylated PLCγ2 inside the cells using PE- PLCγ2 (pY759, BD biosciences). Cells are stained overnight at 4°C. After overnight incubation, each tube of cells is stained with APC-CD56, BV786-CD19, and BUV395-CD3 for 30 minutes at room temperature to identify NK cells and B cells. The cells are washed once with permeabilization buffer and then once with FACS buffer before acquisition using a Cytek Aurora.

The result is represented by the calculated increase of the relative MFI. Relative MFI is calculated by: $\frac{MFI\ of\ NK\ cells\ at\ time\ i}{MFI\ of\ B\ cells\ at\ time\ i}$. The relative MFI at time 0 is the baseline. The calculated increase of the relative MFI is determined by subtracting the baseline from the relative MFI after stimulation.

Table 2.4 Antibodies used for PLCγ2 expression level and phosphorylation assay

Name	Clone	Vendor	Catalogue number
BUV395 Mouse anti-human CD3	SK7	BD biosciences	564001
APC anti-human CD56	5.1H11	Biolegend	362504
PE Mouse anti-PLG-γ2	K86-1161	BD biosciences	560134
PE Mouse IgG1,κ isotype Ctrl	MOPC-21	Biolegend	400111
PE Mouse anti-PLG-γ2(pY759)	K86-689.37	BD biosciences	558490
BV786 Mouse Anti-Human CD19	SJ25C1	BD biosciences	563325

2.6 Antibody titration

5×10^5 PBMCs from the LRS chamber are used as a unit to titrate fluorochrome-conjugated antibodies. 1×10^6 PBMCs are used for viability dye and cell violet tracer titration. The titration of fluorochromes is done by three- or four-fold serial dilution from the recommended usage volume for 1×10^6 cells.

2.7 Statistics

GraphPad Prism 10 is used to do all the statistical calculations. A paired t-test is used to assess the significance of NK cell surface marker expression level, NK cell toxicity difference between samples, and the increase of PLCγ2 phosphorylation level over time.

Chapter 3: Results with HSV+ pediatric patients

Due to the limited number of patient samples and age-matched control samples, we paired two patients with one age matched control and formed three sets according to age and sex (Table 3.1).

Table 3.1 Patient groups of study.

Group	Identifier	Age	Patient or Control	Sex	Notes
Set I	MCIA0362	4	AMC	Female	
	227	7.6	Patient	Female	*HSV1+
	56	1	Patient	Female	HSV1 Keratitis, Encephalitis
Set II	AMC002	3.9	AMC	Male	
	204	4.5	Patient	Male	*HSV1+
	194.1	2.6	Patient	Male	*HSV1+
Set III	MCIA0361	13	AMC	Female	
	174	19	Patient	Female	Cutaneous HSV1
	191.3	12.9	Patient	Female	Cutaneous HSV1

*All the patients are HSV+, but the clinical record were unavailable.

3.1 Cytotoxic activity of patient PBMC

The cytotoxicity assay is performed in 6 patients and 3 age-matched controls (AMC). Cytotoxicity assay is done for each patient and AMC only once in the first round of experiments (Figure 3.1 B-D). Each NK: K562 ratio has duplicates or triplicates according to the cell number.

In the first set, NK cells from patient 227 (Pt227) show significantly lower killing ability compared to the age-matched control (MCIA0362). Patient 56 (Pt56) also has lower NK cytotoxicity ability compared to the age-matched control (AMC) by mean value, but this is not significant. The cytolytic abilities of both the AMC and Pt56 fall into the normal range reported in Alinger (Figure 3.1 E). [12] They are also similar to the cytolytic activity observed in healthy controls in Ornstein's study when the calculated NK: K562 ratio is 1:1.[3]

In the second and third sets of patients, there was no significant difference between healthy controls and patients. However, those healthy controls had very low killing ability compared to MCIA0362 and the healthy range reported in Alinger's paper. This indicates that the results in the second and third sets of killing assays are unreliable, and the killing assay needs to be repeated before doing future functional studies.

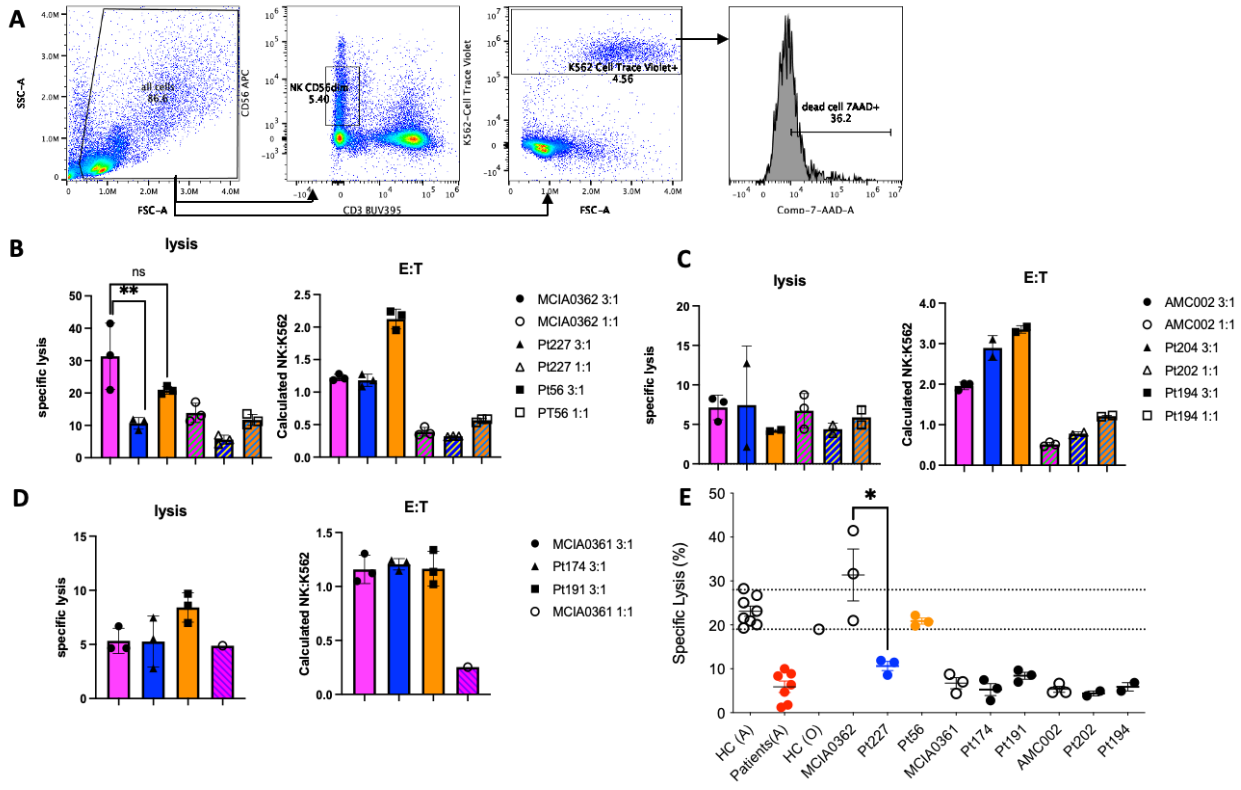

Figure 3.1 Cytotoxicity assay results. A. Gating strategy to get the specific lysis and NK: K562 ratio. $CD56^{dim}$ NK: CD56dim CD3-, K562: Cell trace violet+, lysed K562: 7AAD+. B-D. Specific lysis of K562 in three patient sets. B: set I, C: set II, D: t set III. Magenta is the AMC, blue and orange are the patients. E. Specific lysis of K562 in AMCs and patients in this project and previous works. Open circles are the AMCs. Black or colored dots are patients. Blue represent Pt227, orange represent Pt56 and red represent the pooled patients in Alinger's study. Dashed lines represent the healthy range and drawn according to Alinger's paper[12]. Statistical significance was calculated using paired t test, *P< 0.05, ** P<0.005, ***P<0.001. ****P<0.0001; ns = not significant. Error bars = ±SD.

3.2 PBMC panel and NK cell panel

The 5-laser Cytek Aurora can excite all the fluorochromes and collect the full emission spectrum for those fluorochromes. There are 64 channels in total: 16 channels for UV laser excitation, 16 for violet, 14 for blue, 10 for yellow-green, and 8 for red. This cytometer allows more fluorochromes to be detected simultaneously compared to the FACSCalibur (BD), which was used in Ornstein's study. That cytometer had only two lasers and four channels. Another difference is that the BD FACSCalibur is a conventional flow cytometer, and each fluorochrome needed to be manually compensated. In conventional flow cytometry, all the emitted light has to go through filters that allow only certain wavelengths to pass before they get recorded, while the Cytek Aurora collects the full emission spectrum.

We designed a 19-color immune profiling panel (Figure 3.2 A, Table S2.1) based on a Cytek 25-color Immune Profiling Kit. There are multiple fluorochromes in this panel, so it is possible for the signature peaks of different fluorochromes to be next to each other. Cytek software uses advanced algorithms to unmix the full spectrums, which enables the usage of highly overlapping dyes. For example, APC can be distinguished from Alexa Fluor 647 using spectral flow but not conventional flow. This is not possible with BD Fortessa X-20, even the Fortessa X-20 is one of the most advanced conventional flow cytometers.

Although the Aurora is a powerful tool, one needs to be careful when designing a large immunoprofiling panel. One important guideline is that antigens on the same cell type should be tagged with fluorochromes whose signature peaks are as far away from each other as possible. The two fluorochromes used in the same gating step should be far from each other as well. The other fluorochromes can be closer to each other as long as their expression signatures are unique to each cell type.

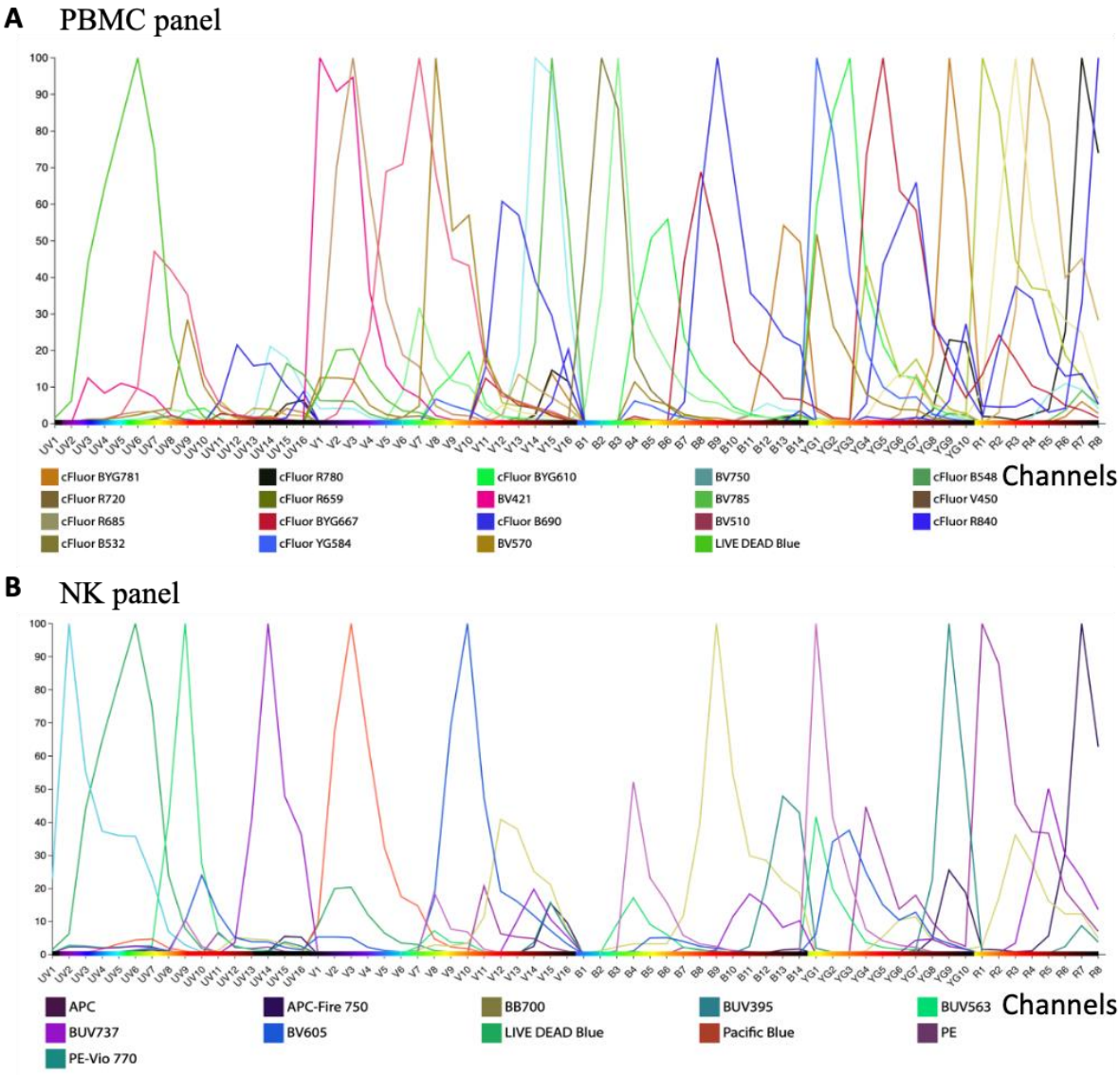

Figure 3.2 Spectral flow panel design. A. Emission spectrum of PBMC panel. B. Emission spectrum of NK panel.

In our 19-color panel, we used some channels right next to each other, for example, the emission peaks of BV510 and BV570 are on channels V7 and V8, BV750 and BV785 are on V14 and V15, and cFluor R685 and cFluor R720 are on R3 and R4. However, in these cases, those fluorochromes are not conjugated to antibodies that target the same kind of cell and are not used in the same gating step. For example, the BV510 is conjugated with IgM antibody to further analyze B cells,

and BV570 is conjugated with CD3 antibody to distinguish NK cells and T cells. In this case, the overlapping of fluorochromes should not cause a problem.

The NK cell surface marker expression and maturation status are acquired by spectral flow using a panel including 11 colors we designed (Figure 3.2 B, Table S2.2). The NK panel has fewer colors, but since we are only focused on NK cells, we must ensure the fluorochromes are dispersed across the whole spectrum, avoiding channels directly next to each other. In this case, the signature peaks of the fluorochromes can be easily distinguished from one another.

3.2.1 PBMC subpopulation

The PBMC subpopulation is shown in Figure 3.3 and the Appendix Table S3. The healthy range reported by Alinger et al is also shown in Table S3.

The samples are pooled together by sex and health status. The healthy range shown in Figure 3.3 is drawn according to Alinger's report[12]. Although he used CyTOF and had different gating strategies, this report is an acceptable reference because we do not have enough age-matched human samples to generate the range. Our female patients and AMCs, on average, have a lower percentage of B cells, mononuclear myeloid cells, and DCs compared to males in our study. Those female patients have a lower percentage of B cells than the male patient in Alinger's study as well. Alinger did not report a DC range, so it is unclear what the healthy range is in the general population, but the mDCs and pDCs are in the lower range in all the AMCs and patients, which is also observed in Alinger's patients.

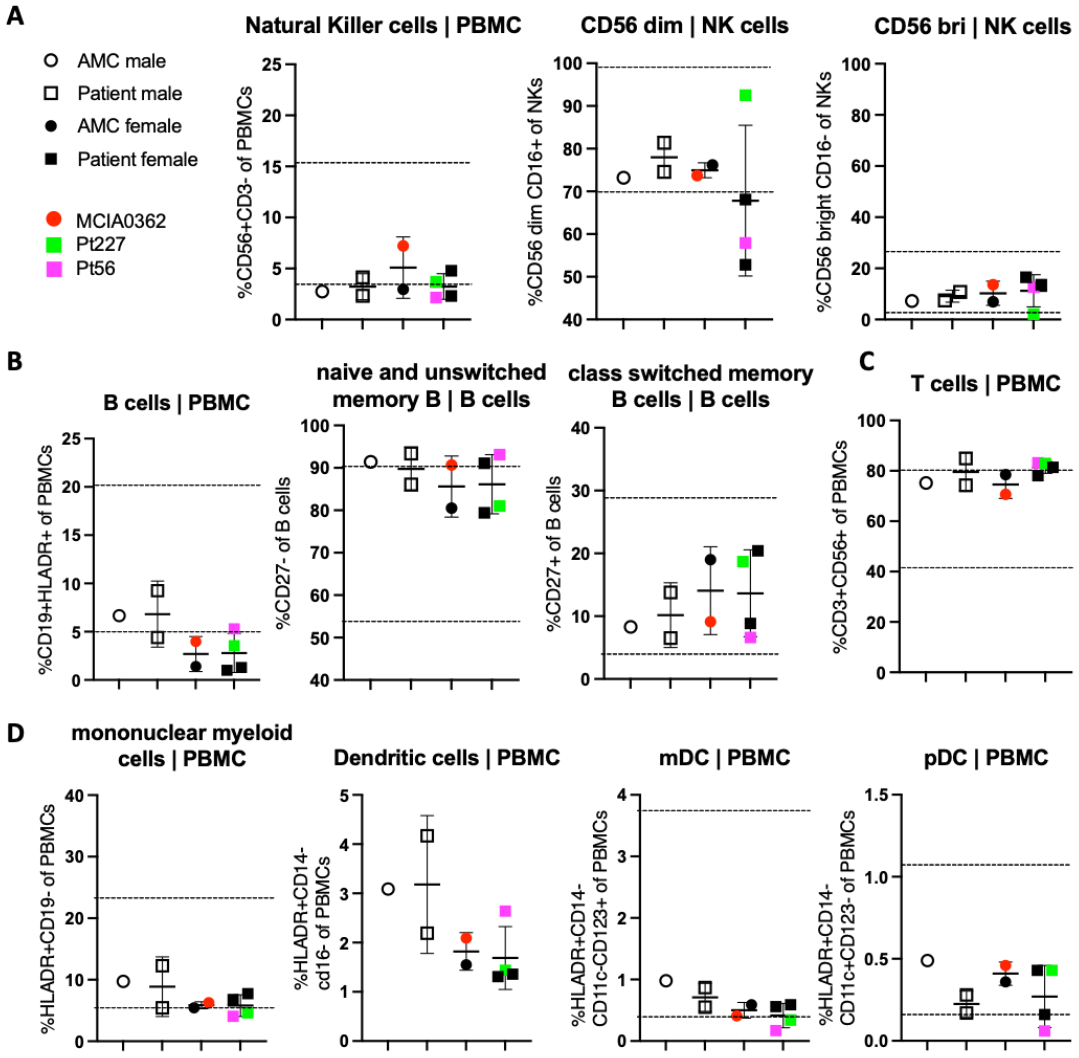

Figure 3.3 Subpopulations of PBMC from all patient samples and AMC. A-D. different subpopulations are quantified and displayed as the percentage of total live PBMCs A. NK cells. Total NK cells (CD3-CD56+), CD56 bright NK cells (CD3-CD16-CD56 bright) and CD56 dim NK cells (CD3-CD16+CD56 dim). B. B cells. Total B cells (HLADR+CD19+), Naïve B cells (HLADR+CD19+IgD+) and class switched memory B cells (HLADR+CD19+IgD-). C. T cells. Total T cells (CD19-CD3+CD56-). D. Mononuclear myeloid cells. Total mononuclear myeloid cells (HLADR+CD19-), pDC (CD16-CD14-CD123+CD11c-), and mDC (CD16-CD14-CD123-CD11c+). The figure legend of all these graphs are the same: open circle represents male AMC, open squares represent male patient, close circles represent female AMC, close squares represent female patient. Red is the AMC in set I (MCIA0362), Green is Pt227 and Magenta is Pt56.

The B cell population in the majority of females is below the healthy range, except Pt56. Pt56 also has a higher naïve and unswitched memory B cell number in all the B cells. The monocyte population in females is on the lower edge of the healthy range. For NK cells, there is no significant difference in the total NK cell population and $CD56^{bri}$ population. However, the average percentage of $CD56^{dim}$ in female patients is lower than the healthy range and has a large variation within the group. $CD56^{dim}$ population in female patients varies from 52.5% (Pt191) to 92.8% (Pt227). Interestingly, Pt227 has the highest $CD56^{dim}$ population, which is characteristic of cytolytic NK cells, but her NK cell demonstrates a functional defect in the cytolytic activity.

3.2.2 NK Cell Panel

The NK panel contains 3 activation markers: CD69, NKG2D, and NKp44; one proliferating marker: Ki67; three stimulatory receptors: NKG2D, NKG2C, NKp44; and two for NK cell maturation: NKG2A and CD57.

The representative 2D tSNE map of the concatenated samples (3 controls and 6 patients) is shown in Appendix Figure S2. The color spectrum represents individual marker-expression levels. CD56, CD11b and NKG2D are expressed on almost all NK cells while CD69, NKG2C and CD57 only expressed on some of the NK cells.

Analysis of expression levels between AMC and patients in the pooled three sets showed no significant differences for NKG2D, NKp44, Ki67, NKG2C, and CD11b (Figure 3.4). The patients have significantly lower CD69 expression, which indicates that their NK cells are not activated even during infection. Except for a decrease in CD69 expression, Pt 56 NK cells are also higher for NKp44 and Ki67 expression, and lower in NK cell number. However, her NK cells kill the target effectively. On the contrary, the expression of NK surface markers in Pt227 is within the range of the AMC, despite the defect in NK killing ability.

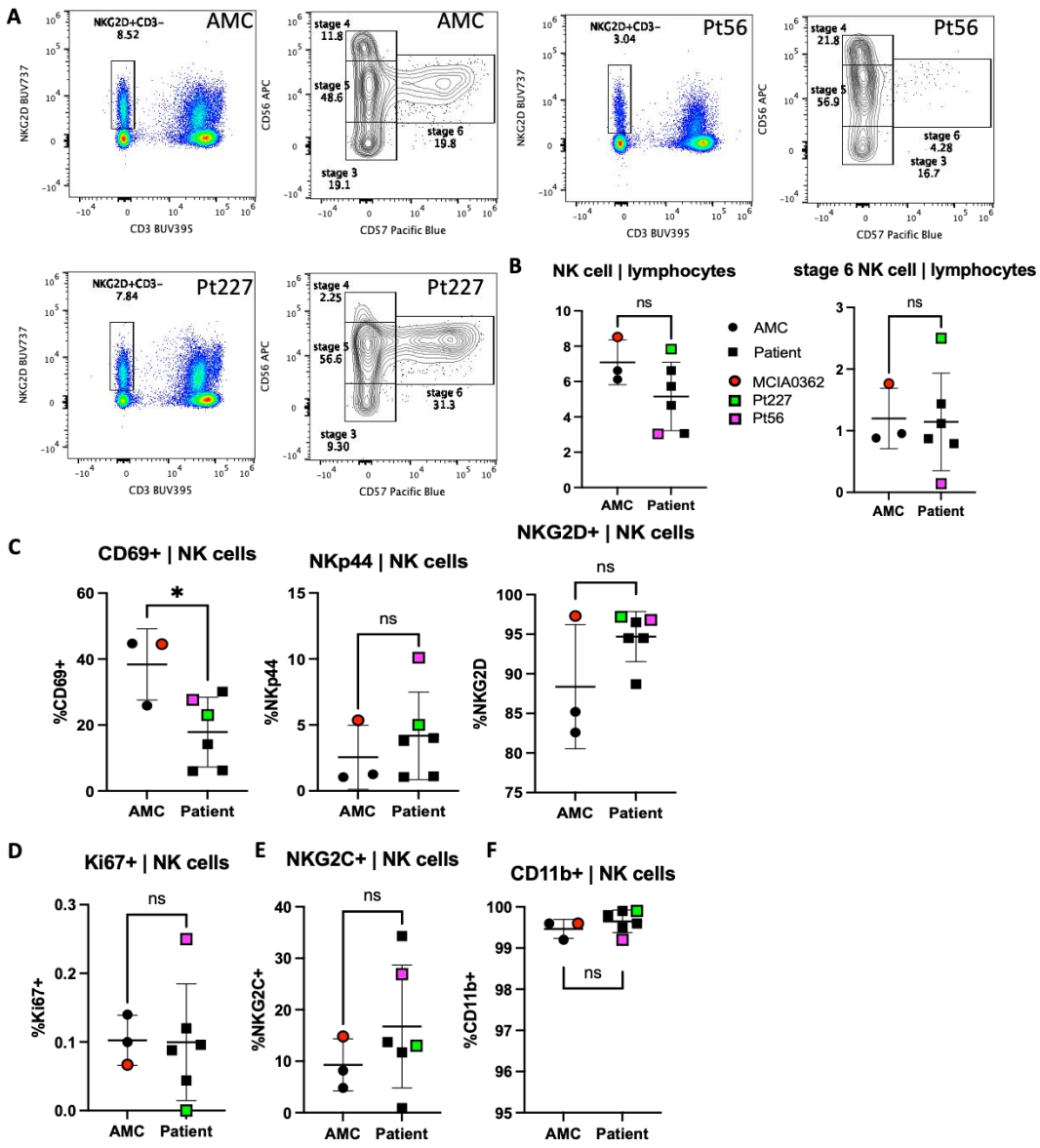

Figure 3.4 NK panel of all patients. A. NK cell maturation status of Patient set I. Total NK gate based on NKG2D+ and CD3-. Stage 3: immature NK, NKG2D+CD56-CD57-; stage 4: CD56^{bri}NK cells: NKG2D+CD56 bright CD57-; stage 5: mature NK, NKG2D+CD56 dim CD57-; stage 6: terminal NK cells NKG2D+CD56 dim CD57+. B. NK cell (NKG2D+CD3-) percentage of all lymphocytes. Round dots are AMC, the red dot is the control showed in A. Squares are the all the patients, the green square is Pt227, and pink square is the Pt56. C-E. NK activation markers, proliferation marker and stimulatory receptors are displayed in a percentage of all NK cells. (C: activation markers; D proliferation marker; E: stimulatory receptors). NKG2D and NKp44 are also stimulatory receptors. F. CD11b expression on all NK cells. Figure legends for C-F are the same as B. Statistical significance was calculated using paired t test, *P< 0.05, ** P<0.005, ***P<0.001. ****P<0.0001; ns = not significant. Error bars = ±SD.

The total $CD56^{dim}$ population in Pt56 NK cells at one year of age is 61.18%, which is close to the 4-year-old age-matched healthy control. Pt227 at 7 years of age has highest number of stage 6 terminal NK cells and has a total of 87.9% $CD56^{dim}$ cells in the NK cell gate ($NKG2D^{+}CD3^{-}$). Although a lot higher than Pt56, the $CD56^{dim}$ NK population for Pt227 still fall within the normal range.

3.3 PLCγ2 expression phosphorylation profiles of Patient Set I

We tested the total PLCγ2 expression on Pt 227, Pt 56, and MCIA0362. Since Pt 227 in Set I had a significantly lower cytolytic ability, we were interested in the PLCγ2 phosphorylation profile for this patient. We analyzed the PLCγ2 phosphorylation on Pt 227 and the age-matched control MCIA0362 using spectral flow. We used CD16 crosslinking to activate the NK cells and measured the change of PLCγ2 phosphorylation level by mean fluorescence intensity (MFI) of phosphorylated PLCγ2 conjugated PE signal in NK cells at different time point after stimulation. The MFI of B cells is used as the internal control since the CD16 crosslinking is specific to NK cells' ADCC pathway, and the baseline PLCγ2 phosphorylation level in B cells is consistent over time. The time of incubation, the amount of fluorochromes, and the machine settings may influence the MFI of both B cells and NK cells. We finally decided to do a two-step normalization. First, calculate the relative MFI of PE in NK cells: $\frac{MFI\ of\ NK\ cells\ at\ time\ i}{MFI\ of\ B\ cells\ at\ time\ i}$. Then consider relative MFI as the baseline and subtract the baseline from stimulated MFI. We can clearly see the total PLCγ2 expression is about the same across all samples in patient set I (Figure 3.5 B), however, Pt227 has a significantly higher PLCγ2 phosphorylation level (Figure 3.5 E).

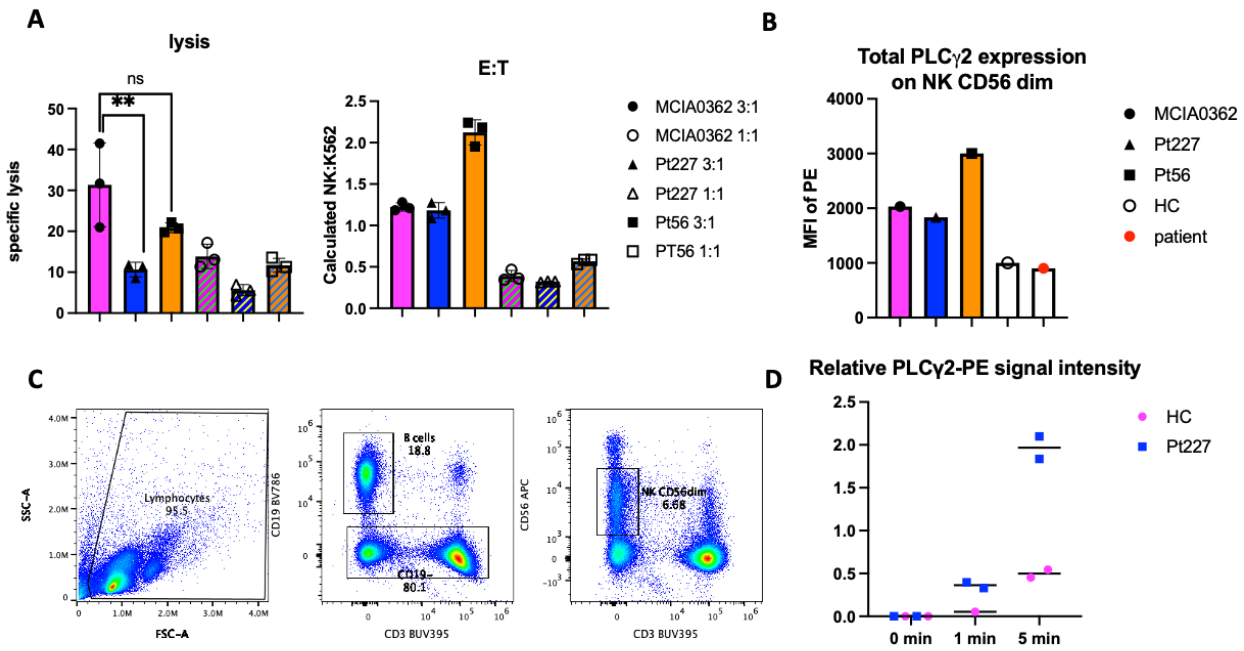

Figure 3.5 Functional assay on sample set I. A. Specific lysis of K562 with AMC and Patient samples. B. total PLCγ2 expression in the age matched control and the two patients in set I. Magenta is the AMC, blue is Pt227, orange is Pt56, blank column with open circle is healthy control reported in Alinger's paper and blank column with red circle dot the patient reported in that paper. The break in x-axis represents the results were collected different date on different machine. C. Gating strategy to identify NK CD56^{dim} cells for PLCγ2 phospho-flow. D. PLCγ2 phosphorylation level in HC and Pt227. The PLCγ2 phosphorylation level is showed by relative PLCγ2-PE signal intensity after stimulation. PBMCs are stimulated by CD16 crosslinking with goat-anti-mouse antibody at 37°C for 0, 1, and 5 minutes. Statistical significance was calculated using paired t test, *P< 0.05, ** P<0.005, ***P<0.001. ****P<0.0001; ns = not significant. Error bars = ±SD.

3.4 Discussion

One out of 6 patients studied (Pt227) has significantly lower cytolytic activity compared to the age- and sex-matched healthy control. The AMC in sets II and III, were unable to lyse targets, making the results for those patient pairs inconclusive. Some of the AMC samples were collected during or after the COVID-19 pandemic, which may have influenced these studies. As well, there may have been problems with some of the experimental reagents. All assays will be repeated for those sets once new AMC are verified for cytolytic activity. We were able to run only one experiment for each patient sample, so the following conclusions are preliminary and repeat experiments are needed to understand the phenotypes of those patients more clearly.

The PBMC and NK panel profiles as well as total PLCγ2 expression do not differ between Pt227 and the AMC. However, the surprising feature of Pt227 is that she has significant PLCγ2 hyperphosphorylation in response to CD16 crosslinking despite lower NK cytolytic activity. This feature is unexpected and does not correlate to Alinger's study, showing the relationship between low cytolytic activity and PLCγ2 hypophosphorylation. One possible reason for the hyperphosphorylation of PLCγ2 but low NK cytolytic function is that Pt227 may have some problems with other upstream or downstream signaling molecules like Lck and ERK or a PLCγ2 mutation in another region leading to this unexpected phenotype. Alinger et al is the only published report that shows a relationship between NK cell functional defects of PLCγ2 haploinsufficiency. This current project is set to be a continuing study of possible NK functional defects due to PLCγ2 defects. The unexpected finding of hyperphosphorylation of PLCγ2 in Pt227 calls for more investigation with pediatric HSV patients.

Another interesting feature of Pt227 is that she has a lot more terminally mature NK cells compared to the AMC and every other patient included in the study. This result correlates to patients A.II.3 and B.II.4 in Alinger's study, who had an increase in mature NK cells and loss of killing function. Although cytolytic activity for Pt56 fell into the normal range it is still an interesting sample. Pt56 has significantly lower B cells, NK cells, monocytes, pDCs, and mDCs counts across the board, which may contribute to recurrent infections. She also has a very low number of terminal and memory-like NK cells, which may be due to her age of 1 year. Also, she has significantly higher NKp44 and Ki67 expressions, which indicates that her NKs were activated and proliferating at the time of the blood draw. Ki67 is also related to high serum IL-15 and increased $CD56^{bri}$ population.[22] According to Alinger's study, the function of NK cells after expanding on an irradiated K562-mbIL-15-41BB/IL-2 feeder layer IL-15 is restored to AMC level regarding

calcium flux and cytolytic ability. It is possible that the high Ki67 expression on NK cells is also related to high IL-15 and a restored NK function. Although our lab did not measure the IL-15 level at the time of the blood draw, we can consider this in future studies.

There are some interesting features of other patients as well. For example, Pt191 has a normal PBMC immune profile and normal surface marker expression except her NK cell CD56 bright and dim populations differ from the average. In general populations, the $CD56^{bri}$: $CD56^{dim}$ ratio is usually around 1:10 or lower.[23] However, in Pt191, this ratio is almost 1:2, which indicates her NK cells are not fully mature. However, she has a population of $CD56^{bri}CD16^{+}$ which is very low in number in general populations. A previous study found $CD56^{bri}CD16^{+}$ NK cells are intermediates in phenotype and function and these cells have cytolytic ability[24], so we cannot predict how well her NK cell can lyse target. Similarly, Pt194 also has a higher $CD56^{bri}$ population. The $CD56^{bri}$ to $CD56^{dim}$ ratio is 1:5 in his NK cells, so his sample is worth further study.

After one year of honing skills to master spectral flow cytometry and learn to set up functional assays, we had an unfortunate issue with AMCs. The NK cytolytic assays for two out of three patient sets were inconclusive because the AMC did not show lysis of targets as expected. We tried to troubleshoot but could not resolve the problem. At this time, we are halting all patient sample studies until all possible problems are solved and new AMCs are confirmed with normal cytolytic ability.

For future continuing studies to this project, more patients with severe HSV infection need to be included. Similar NK and PBMC panels and the cytolytic assay will still be the first tier of experiments. PLCγ2 phenotypes, including total PLCγ2 expression and PLCγ2 phosphorylation will be studied in patients with killing defects.

The future study on Pt56 should be carried out on samples from another blood draw at 4.7 years of age. We would expect to see similar PBMC profiles and possibly increased terminal NK populations due to more NK memory cells accumulated over time. We are interested in whether the NKp44 and Ki67 expression levels of that 4.7-year-old sample drop back to the normal range and whether there will be an NK killing defect in that patient sample.

Planned future studies for Pt227, who showed functional NK defects, would be to repeat the cytolytic assay in addition to the PLCγ2 phosphorylation study to see whether the NK PLCγ2 hyperphosphorylation phenotype is repeated. If so, this would be an interesting novel finding. It would also be useful to simultaneously set up B cell PLCγ2 phosphorylation in response to IgM stimulation.

Chapter 4: Results with LRS chambers and the troubleshooting

4.1 PBMC viability tracking

IL-15 is a cytokine that is not secreted by NK cells, but it can regulate NK cells. It can significantly activate NK cells and increase NK cell cytotoxicity at 10 ng/ml.[25] It can also help NK cell expansion in vitro, but long-term treatment of IL-15 can exhaust NK cells.[26,27] However, a low dose of IL-15 can help maintain NK viability.

The viability of PBMC over time under various conditions is shown in Figure 4.1. The percentage of dead PBMC is consistent with different culture times and different reagents, except for the fresh thawed PBMC. PBMC death increases over time. After 1h incubation at 37°C all cells have high viability. After 4 hours, viability decreases. For overnight incubation with low dose IL-15, the effect in maintaining cell viability between 3 ng/ml and 5 ng/ml is almost the same. When the IL-15 concentration is the same, increasing the serum percentage in the culture media did not help PBMC viability. In general, culturing the primary cells overnight leads to lower viability of total PBMCs and lymphocytes. Although the percentage of live lymphocytes after the overnight incubation with RPMI with 15% FCS and 3 ng/ml IL-15 is almost the same as those rested for only one hour, the other compartment of PBMCs or monocytes and granulocytes were dying by the second day, which may introduce more auto-fluorescence in the flow cytometry run. We concluded all the functional tests should be performed with freshly thawed PBMC after one hour of rest at 37°C.

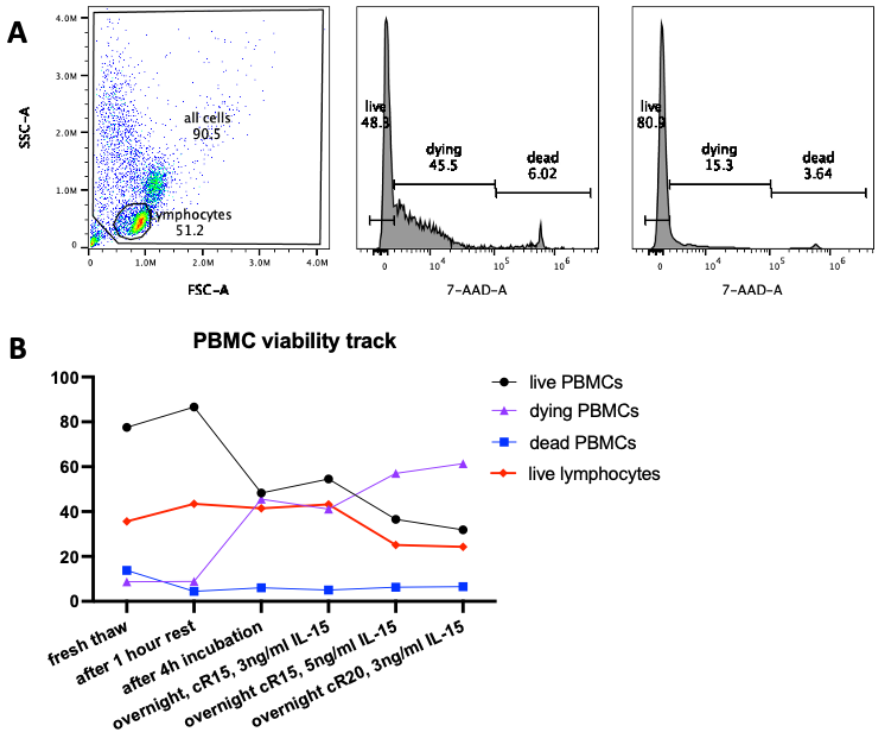

Figure 4.1 PBMC viability track after thaw. A. Gating strategy for viability track. 7AAD intensity is used to mark the PBMC viability after thaw over time. The live cell gate is settled according to the negative peaks of PBMC(<$1.1x10^3$). The dead cell gate is settled according to the positive 7AAD control (> $1x10^5$). The cells whose signal intensity is between $1.1x10^3$ and $1x10^5$ are categorized as dying cells. B. Viability of PBMC. The live PBMCs are showed by black dots, the dying PBMCs are showed by purple triangles, the dead PBMCs are showed by blue squares and the live lymphocytes are showed in red diamonds.

4.2 PBMC immunoprofiling with LRS chamber and troubleshooting

4.2.1 Fluorochrome conjugated antibody titration

To optimize the staining condition to make sure the fluorochromes stain significantly and specifically, we did fluorochrome-conjugated antibody titration for CD56 BV750 (Biolegend), CD3 BV570 (Biolegend), PD-1-BV785 (Biolegend), IgM BV510 (Biolegend), and CD16-PE/Dazzle 594 (Biolegend) for the PBMC panel; CD19-BV786 (BD biosciences), CD56-APC (Biolegend), and CD3-BUV395 (Biolegend) for cytolytic assay. The viability dye Live/Dead Blue

is also titrated but with 1×10^6 PBMCs after PBS wash. The titration results are shown in Appendix Table S4.

4.2.2 Trouble shooting Spectral flow unmixing issues using LRS chamber

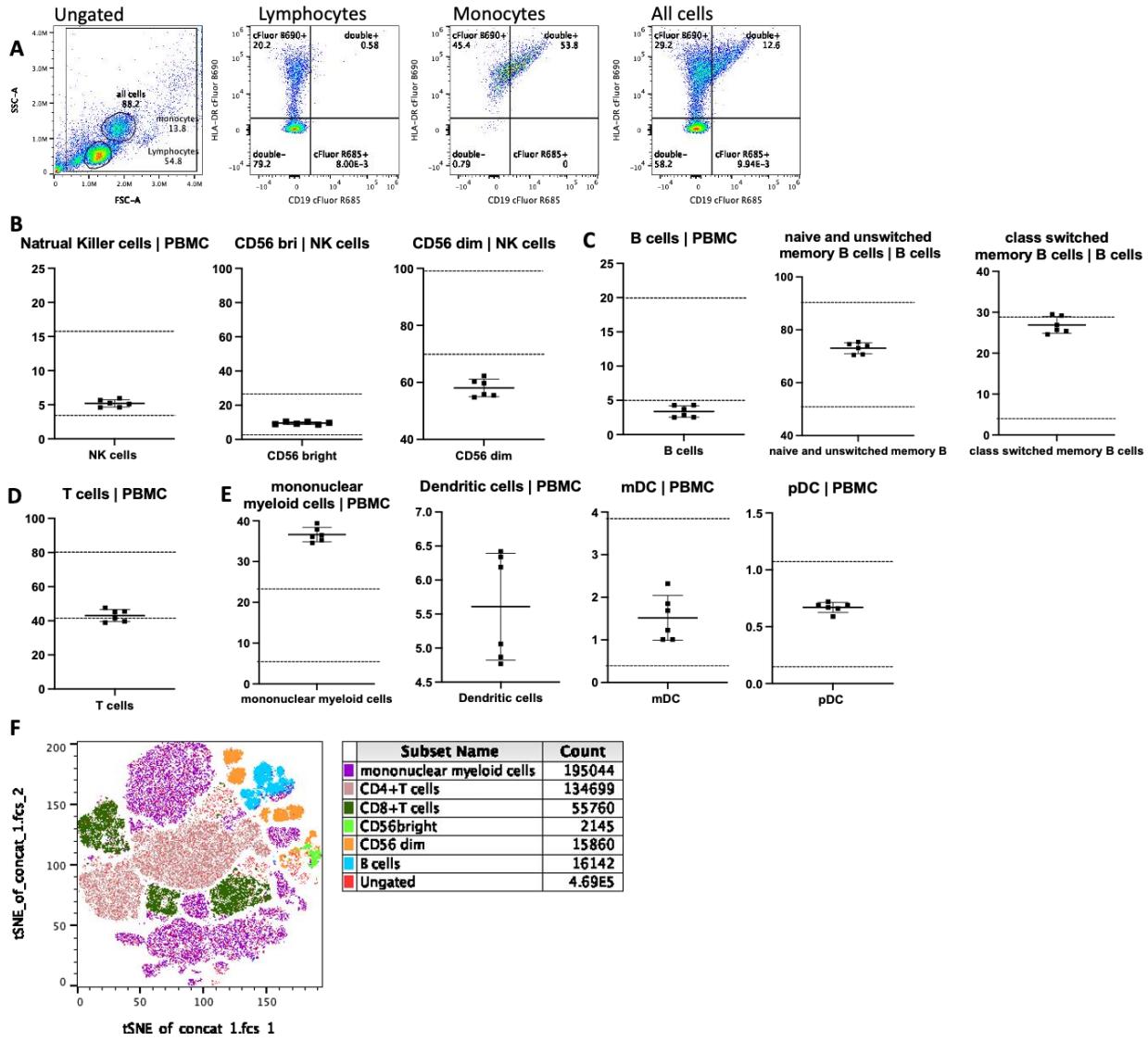

Figure 4.2 PBMC subpopulation in the 05/17/23 LRS chamber. A. Unmixing problem with the single-color reference. B-E. Confirming staining patterns of PBMC using LRS chamber. B. NK cells. Total NK cells (CD3-CD56+), CD56 bright NK cells (CD3-CD16-CD56 bright) and CD56 dim NK cells (CD3-CD16+CD56 dim). C. B cells. Total B cells (HLADR+CD19+), Naïve B cells (HLADR+CD19+IgD+) and class switched memory B cells (HLADR+CD19+IgD-). D. T cells. Total T cells (CD19-CD3+CD56-). E. Mononuclear myeloid cells. Total mononuclear myeloid cells (HLADR+CD19-), pDC (CD16-CD14-CD123+CD11c-), and mDC (CD16-CD14-CD123-CD11c+). F. 2D tSNE plot of the concatenated 05/17/23 LRS. The plot is overlayed with NK CD56dim, NK CD56bri, B, CD4+T, CD8+ T, mononuclear myeloid cells.

With the experiments using PBMC from LRS chambers, we found there were some problems with signal compensation between HLA-DR cFluor B690, CD16 cFluor BYG610, and CD19 cFluor R685. The compensation problem was first found in the single-color control of CD19 cFluor R685. When including both mononuclear myeloid cells and lymphocytes, the positive population of cFluorB690 spreads out. If we narrowed down the gate to lymphocytes, the positive population in the single-color control aligns properly above the negative population, and if we narrow down the gate to monocytes according to the forward scatter and side scatter, we can clearly see that the majority of cells tilt to the right and become pseudo-double positive, indicating an unmixing problem (Figure 4.2 A). This problem comes from the fluorescence leak from cFluor B690 into the R3 channel. When this single-color positive control was recorded and set as the positive control, the intensity in R3 was decreased. Because we have a limited amount of fluorochrome that is not enough to accompany single color control for every single experiment, we decided to do manual unmixing in FlowJo program with these two fluorochromes after the Cytek software calculated for the others in the panel.

The PBMC panel practice runs using the same LRS chamber were repeated 6 times. This LRS chamber has significantly more mononuclear myeloid cells and fewer T cells than the healthy range reported in Alinger's study. The populations we are interested in studying are NK cells and B cells. These subpopulations do not display variation between runs. The experimental setup is a critical learning tool for processing samples. These are to ensure the reproducibility of the results, to show the antibody titration is correct, and to confirm the designed panel is practical and reliable before analyzing the actual patient samples.

4.3 NK Panel on LRS chamber and troubleshooting

As aforementioned, NKp44 and Ki67 are not expressed on resting NK cells. To prepare the single-color positive controls for these two fluorochrome-conjugated antibodies, we tried different stimulation methods including different concentrations of IL-2 with different times of co-incubation and we also tried PMA stimulation. The result is shown in Appendix Table S5.

We added NKG2A into the panel as a representation of NK maturation status. $NKG2A^{-}CD57^{-}$ NK cells are the most naïve NK cells and then NKG2A starts to express on $CD56^{bri}$ NK cells. Then, NKG2A expression drops and CD57 expression rises as the NK cells mature to finally become terminally mature, characterized by $NKG2A^{-}CD57^{+}$ expression. However, we observed some problems with our NKG2A staining within the panel. We looked back at the panel design and found no fluorochrome overlapping and the single-color references did not show any leakage on other channels. We sought to find whether the problem came from competition between the conjugated antibodies. To find out whether this is the problem, we set up three smaller panels so we could follow up on Alinger's findings. All of them show a fair amount of expression of NKG2A so I concluded that CD56, CD3, CD57, NKG2C, and LDB do not influence the staining of NKG2A. We then used this set of fluorochromes for common staining and screened the other fluorochromes in the panel by the full minus one (FMO) strategy. Unfortunately, none of them showed a positive signal for NKG2A. We repeated the FMO screening and used only CD56, CD3, and NKG2A as the common staining panel. We found only the group without CD57 was able to show a positive signal of NKG2A. This indicated that it is the CD57 antibody and some other antibodies together affecting the staining pattern of NKG2A. Instead of delving into the further study of which particular fluorochrome is influencing the staining, we decided to not use NKG2A as the marker for maturation studies. We know that the NKG2D starts to express earlier than

NKG2A and CD56, and CD56 becomes bright when NKG2A starts to express. CD56 gets dim when NKG2A expression decreases and keeps dim when CD57 starts to express. So, we decided to present the maturation status of NK cells in another way (Figure 4.3 A). First gating on $NKG2D^{+}CD3^{-}$ for NK cells. And then looking at CD56 versus CD57 profiles for maturation. Immature NK cells are defined as the $CD56^{-}CD57^{-}$ cells, and $CD56^{bri}$ NK cells are $CD56^{bri}CD57^{-}$ cells. $CD56^{dim}$ $CD57^{-}$ is the marker of the mature NK cells and once NK cells are terminally mature, they gain CD57 expression and become $CD56^{dim}CD57^{+}$.

The NK panel profiles of LRS chambers are shown in Figure 4.3. The NK cell percentage in LRS1 (12/12/23) is higher than the normal range (5-15%). The LRS2 (02/16/22) and LRS3 (05/19/23) are within the normal NK cell range. However, the NK cells maturation status of LRS2 is different from the other two. It has significantly higher stage 6 NK cells and lower stage 4. The LRS2 NK cells cannot lyse targets as well as the other two LRS chambers, which correlates with the Pt227 mentioned in Chapter III and the patient A.II.3 studied by Alinger et al. The LRS chambers come from different blood donors. They are usually healthy males, but their actual health status, sex, and race are protected information. So, these experiments with the LRS chambers are not for conclusion but rather to ensure consistency in experimental design.

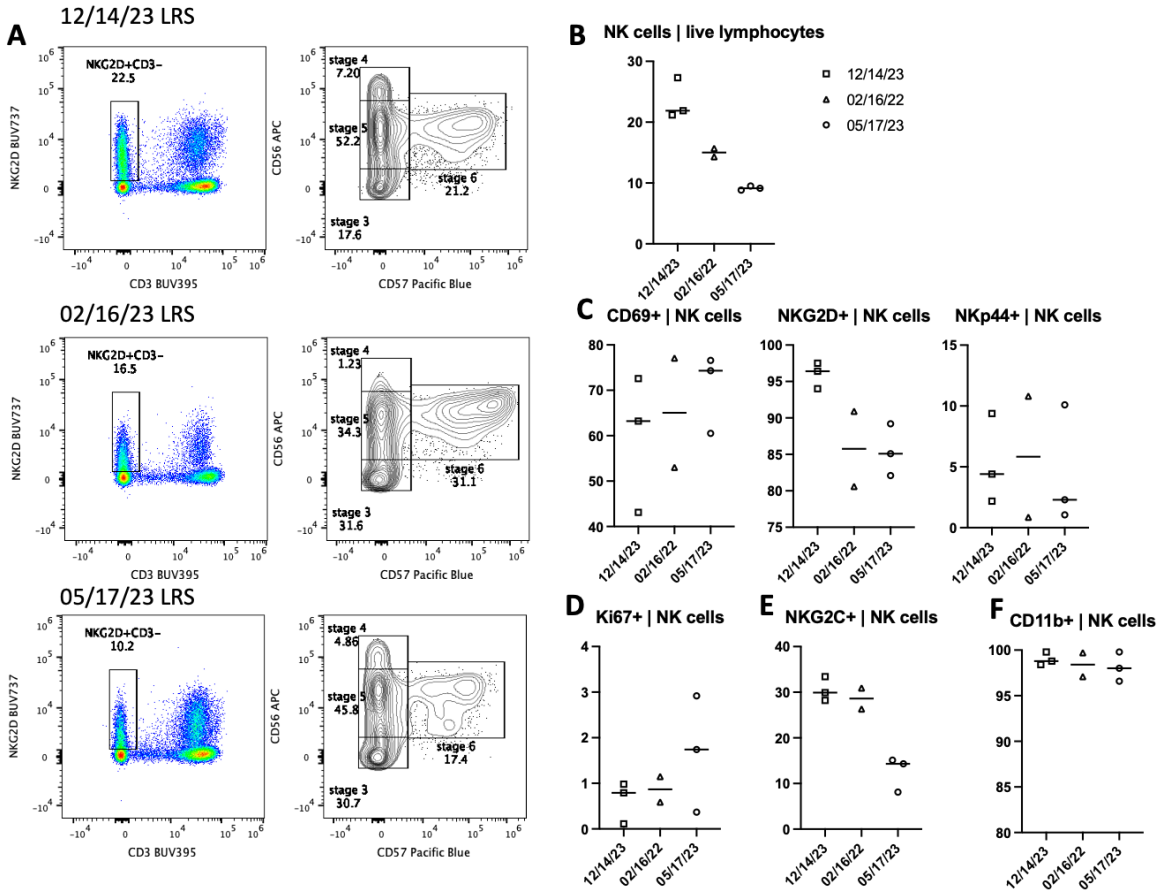

Figure 4.3. NK panel of 3 different LRS chambers. A. NK cell maturation state of three different LRS chambers. Total NK gate based on NKG2D+ and CD3-. Stage 3: immature NK, NKG2D-/+CD56-CD57-, stage 4: CD56^{bri} NK, NKG2D+CD56 bright CD57-, stage 5: mature NK, NKG2D+CD56 dim CD57-, stage 6: terminal NK cells NKG2D+CD56 dim CD57+. B. NK cell (NKG2D+CD3-) percentage of all lymphocytes. Square is the PBMC from 12/14/23 LRS chamber, Triangle is from 02/16/22 LRS and circle is from 05/17/23. C-E. NK activation markers, proliferation markers stimulatory receptors are displayed in a percentage of all NK cells. (C: activation; D proliferation; E: stimulatory receptors). NKG2D and NKp44 are also stimulatory receptors. F. CD11b expression on all NK cells. Figure legends for C-F are the same as B.

4.4 Cytolytic assay on LRS chambers

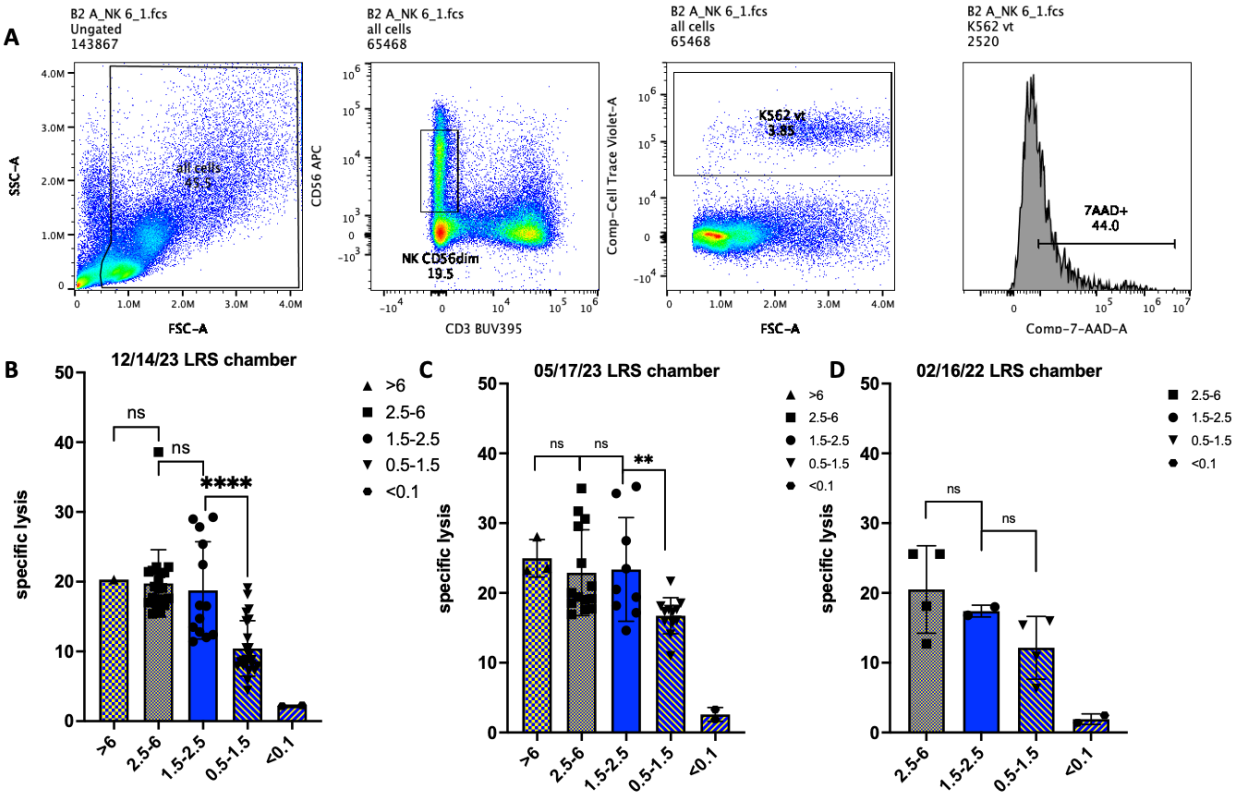

Figure 4.4 Cytotoxicity analysis of LRS chambers. A. Gating strategy to identify K562s and NK cells in the assay. PBMCs are labeled with CD56-APC and CD3-BUV395, and K562s are stained with Cell Violet Tracer. Lysed K562 are labeled by 7AAD. B-D. Specific lysis of K562 after co-culture with PBMC from different LRS chamber. B. 8 replicates for 12/14/23 LRS chamber. C. 7 replicates for 05/17/23 LRS chamber. D. 3 replicates for 02/22/24 LRS chamber. Y-axis: specific lysis. X-axis: calculated E: T range. Statistical significance was calculated using paired t test, *P< 0.05, ** P<0.005, ***P<0.001. ****P<0.0001; ns = not significant. Error bars = ±SD.

The cytotoxicity assay is done in three different LRS chambers (Figure 4.4), the cytolytic ability varies among cells, but all those NK cells lyse more than 15% of targets when the calculated NK to K562 ratio is around 2. NK cell lysis of targets decreased to around 15% when the NK to K562 ratio decreased to around 1 for the 12/14/23 and 5/17/23 LRS chambers. Due to the limited number of 02/16/22 LRS I have, I only did three experiments in duplicate with this LRS chamber. The decrease in specific lysis for the 2/16/22 LRS chamber is not significant between different E:T ratios. Fewer data points may contribute to this result.

4.5 Degranulation assay practice on LRS chambers

The degranulation assay was not included in our first tier of patient studies because previous works in our lab showed normal degranulation (by CD107a) in NK cells despite lower cytolytic ability in patients. We decided to wait to study the degranulation phenotype in human samples until we find data that indicates defects in patient NK function. However, to prepare, I learned and practiced the degranulation assay several times using LRS chambers.

4.5.1 Methods of degranulation assay

Human K562 tumor cells are used as targets in this NK cell degranulation assay. PBMCs from LRS are thawed and rested for one hour at 37°C in cR10. 5×10^5 PBMC are plated into 96-well U-bottom plate with or without 1000 U/ml IL-2 and K562 at a PBMC-K562 ratio of 1:1. After one hour of co-culture at 37°C in Heracell™ VIOS 160i CO2 Incubator, 0.3 μl Golgi-stop (BD biosciences) is added to each well and cultured for three more hours. Cells in the plate are washed twice and then labeled with APC-CD56 (Biolegend), BUV395-CD3 (BD biosciences), and CD107a-PE (BD biosciences) to identify NK cells degranulation. The percentage of NK cells and the degranulation profiles of NK cells are collected using a Cytek Aurora.

4.2.3 Result of NK cell degranulation using LRS chambers

The degranulation assay is done using two LRS chambers (Figure 4.5). The PBMCs from the 05/17/23 LRS chamber have an average degranulation baseline of 15%, and after 4 hours of co-incubation with K562 and 1000 U/ml IL-2, it increases to 40%. In the 12/14/23 LRS chamber, the average degranulation baseline was 20% and increased to more than 40% after stimulation with K562 and IL-2.

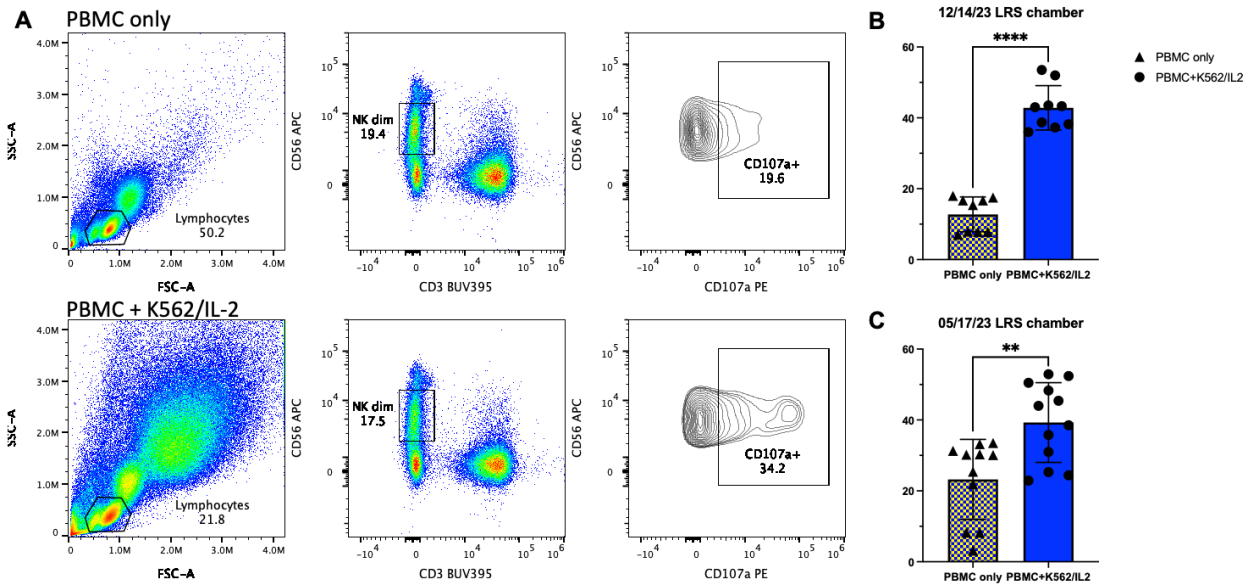

Figure 4.5. Degranulation analysis of LRS chambers. A. Gating strategy to identify CD107a+NK cells in the assay. PBMCs are labeled with CD56-APC and CD3-BUV395, and CD107a is labeled with PE. B-C. Pooled degranulation level of NK after 4 hours co-culture. B. 12/14/23 LRS chamber. Singlet or duplicate each time (n=5). C. 05/17/23 LRS chamber. Singlet or duplicate each time (n=6). Statistical significance was calculated using paired t test, *P< 0.05, ** P<0.005, ***P<0.001. ****P<0.0001; ns = not significant. Error bars = ±SD.

4.6 PLCγ2 expression and phosphorylation on LRS chambers

4.6.1 Result of PLCγ2 expression

We measured the PLCγ2 expression on CD56^{dim} NK cells by mean fluorescence intensity (MFI). The two healthy donors have different total PLCγ2-PE signal intensities. One at 6000 and the other at 1000 on different days. The PLCγ2 phosphorylation was measured by relative MFI of PE increase at different time points of CD16 stimulation.

4.6.2 Optimization of the protocol to measure PLCγ2 phosphorylation

We found with the previous protocol, the MFI of pPLCγ2-PE in B cells increased as the CD16 stimulation time course. We tried two different ways to solve this problem. First, we added an Fc block step before CD16 stimulation. Second, we moved the step for NK cell and B cell surface staining from the beginning of the setup to after the permeabilization. This solved the background

problem we were seeing in the B cell profiles. This troubleshooting was important because the MFI in B cells was used as an internal reference to determine NK cell PLCγ2 phosphorylation.

4.2.3 Result of PLCγ2 phosphorylation

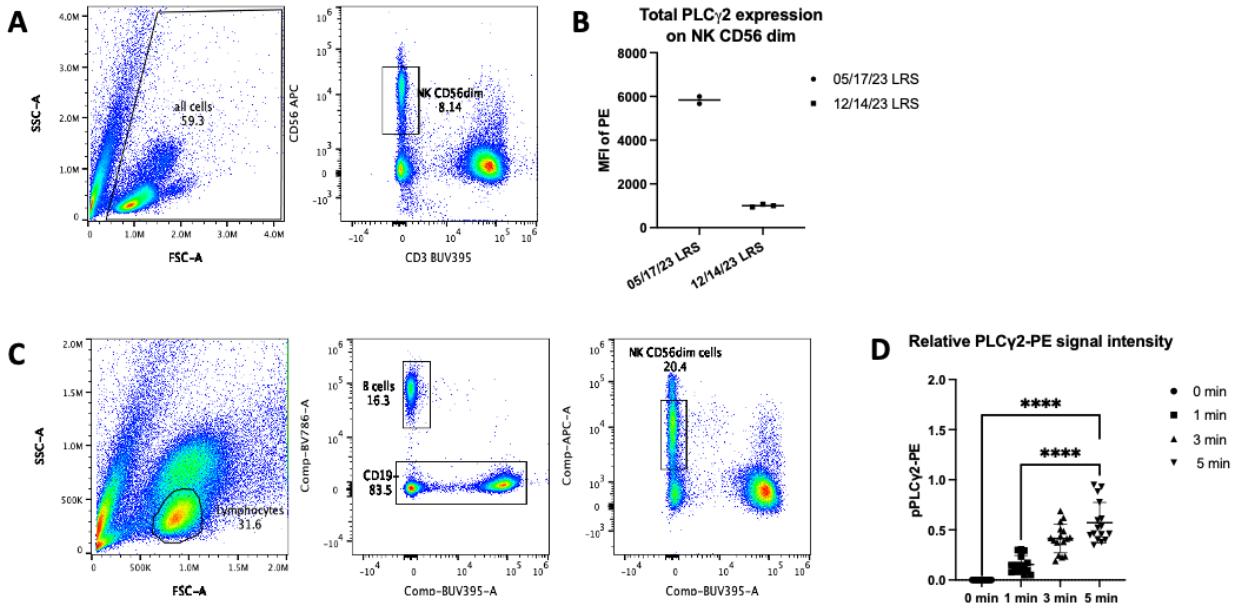

Figure 4.6 Total PLCγ2 expression and PLCγ2 phosphorylation. A. Gating Strategy for PLCγ2 expression on NK cells. B. Total PLCγ2 expression level of two LRS chambers processed from two different dates. C. Gating Strategy for PLCγ2 phosphorylation on CD56 dim NK cells. D. Normalized PLCγ2 phosphorylation level by relative phosphorylation level in 12/14/23 LRS.

Once we were able to troubleshoot the issue above, we proceeded to practice this assay using LRS chambers. The result is shown in Figure 4.6 D. The relative pPLCγ2-PE intensity increases from around 1 to around 1.6, so we subtracted the relative pPLCγ2-PE intensity at time 0 from the rest, yielding a relative PLCγ2-PE intensity increases of 0.57 on average after 5 minutes of CD16 crosslinking. The average increase after 1 minute of stimulation is 0.155 and that after 3 minutes of stimulation is 0.415. The increase is significant in this five-minute range.

References

1. Sukik, L., Alyafei, M., Harfouche, M. & Abu-Raddad, L. J. Herpes simplex virus type 1 epidemiology in Latin America and the Caribbean: Systematic review and meta-analytics. *PLOS ONE* **14**, e0215487 (2019).

2. Schulte, J. M. *et al.* HSV-1 and HSV-2 Seroprevalence in the United States among Asymptomatic Women Unaware of Any Herpes Simplex Virus Infection (Herpevac Trial for Women). *South. Med. J.* **107**, 79–84 (2014).

3. Ornstein, B. W., Hill, E. B., Geurs, T. L. & French, A. R. Natural Killer Cell Functional Defects in Pediatric Patients With Severe and Recurrent Herpesvirus Infections. *J. Infect. Dis.* **207**, 458–468 (2013).

4. Favier, B., LeMaoult, J., Lesport, E. & Carosella, E. D. ILT2/HLA-G interaction impairs NK-cell functions through the inhibition of the late but not the early events of the NK-cell activating synapse. *FASEB J.* **24**, 689–699 (2010).

5. Cooper, M. A., Fehniger, T. A. & Caligiuri, M. A. The biology of human natural killer-cell subsets. *Trends Immunol.* **22**, 633–640 (2001).

6. Della Chiesa, M. *et al.* Human NK Cells and Herpesviruses: Mechanisms of Recognition, Response and Adaptation. *Front. Microbiol.* **10**, 2297 (2019).

7. Paul, S. & Lal, G. The Molecular Mechanism of Natural Killer Cells Function and Its Importance in Cancer Immunotherapy. *Front. Immunol.* **8**, 1124 (2017).

8. Koch, J., Steinle, A., Watzl, C. & Mandelboim, O. Activating natural cytotoxicity receptors of natural killer cells in cancer and infection. *Trends Immunol.* **34**, 182–191 (2013).

9. Román, V. R. G., Murray, J. C. & Weiner, L. M. Chapter 1 - Antibody-Dependent Cellular Cytotoxicity (ADCC). in *Antibody Fc* (eds. Ackerman, M. E. & Nimmerjahn, F.) 1–27 (Academic Press, Boston, 2014). doi:https://doi.org/10.1016/B978-0-12-394802-1.00001-7.

10. Kruse, P. H., Matta, J., Ugolini, S. & Vivier, E. Natural cytotoxicity receptors and their ligands. *Immunol. Cell Biol.* **92**, 221–229 (2014).

11. Orange, J. S. Natural killer cell deficiency. *J. Allergy Clin. Immunol.* **132**, 515–525 (2013).

12. Alinger, J. B. *et al.* Human PLCG2 haploinsufficiency results in a novel natural killer cell immunodeficiency. *J. Allergy Clin. Immunol.* S0091674923011430 (2023) doi:10.1016/j.jaci.2023.09.002.

13. Arneson, L. N. & Leibson, P. J. Signaling in Natural Immunity: Natural Killer Cells. in *NeuroImmune Biology* (eds. Bertók, L. & Chow, D. A.) vol. 5 151–166 (Elsevier, 2005).

14. Prole, D. L. & Taylor, C. W. Structure and Function of IP $_3$ Receptors. *Cold Spring Harb. Perspect. Biol.* **11**, a035063 (2019).

15. Chakraborty, P. *et al.* Regulation of store-operated Ca2+ entry by IP3 receptors independent of their ability to release Ca2+. *eLife* **12**, e80447 (2023).

16. Milner, J. D. PLAID: a Syndrome of Complex Patterns of Disease and Unique Phenotypes. *J. Clin. Immunol.* **35**, 527–530 (2015).

17. Bunney, T. D. *et al.* Structural and Functional Integration of the PLCγ Interaction Domains Critical for Regulatory Mechanisms and Signaling Deregulation. *Structure* **20**, 2062–2075 (2012).

18. Ombrello, M. J. *et al.* Cold Urticaria, Immunodeficiency, and Autoimmunity Related to PLCG2 Deletions. *N. Engl. J. Med.* **366**, 330–338 (2012).

19. Baysac, K. *et al.* PLCG2-associated immune dysregulation (PLAID) comprises broad and distinct clinical presentations related to functional classes of genetic variants. *J. Allergy Clin. Immunol.* **153**, 230–242 (2024).

20. Belkina, A. C. *et al.* Automated optimized parameters for T-distributed stochastic neighbor embedding improve visualization and analysis of large datasets. *Nat. Commun.* **10**, 5415 (2019).

21. Linderman, G. C., Rachh, M., Hoskins, J. G., Steinerberger, S. & Kluger, Y. Fast interpolation-based t-SNE for improved visualization of single-cell RNA-seq data. *Nat. Methods* **16**, 243–245 (2019).

22. Hudspeth, K. *et al.* Natural killer cell expression of Ki67 is associated with elevated serum IL-15, disease activity and nephritis in systemic lupus erythematosus. *Clin. Exp. Immunol.* **196**, 226–236 (2019).

23. Mahapatra, S. *et al.* High-resolution phenotyping identifies NK cell subsets that distinguish healthy children from adults. *PLOS ONE* **12**, e0181134 (2017).

24. Béziat, V. *et al.* CD56brightCD16+ NK Cells: A Functional Intermediate Stage of NK Cell Differentiation. *J. Immunol.* **186**, 6753–6761 (2011).

25. Carson, W. E. *et al.* Interleukin (IL) 15 is a novel cytokine that activates human natural killer cells via components of the IL-2 receptor. *J. Exp. Med.* **180**, 1395–1403 (1994)

26. Felices, M. *et al.* Continuous treatment with IL-15 exhausts human NK cells via a metabolic defect. *JCI Insight* **3**, (2018).

27. Lu, X., Liu, J., Zhuxia, J., Ouyang, X. & Chen, B. Selectively and Efficiently Expanding Natural Killer Cells in Vitro. *Blood* **136**, 20–20 (2020).

Appendix

Table S1. Reagents

Reagent	Company	Catalogue number
Brilliant stain buffer plus	BD biosciences	566385
RPMI 1640	Sigma-Aldrich	R8758-1L
Fetal Calf Serum	ThermoFisher Scientific	A5256701
sodium pyruvate	Corning	25-000-CI
MEM nonessential amino acids	Corning	25-025-CI
HEPES buffer	Corning	25-060-CI
Penicillin-Streptomycin	ThermoFisher Scientific	15070063
2-mercaptoethanol	ThermoFisher Scientific	A5256703
10x Sterile PBS	Einco Technologies, Inc.	P349
PBS	Corning	21-040-CM
HBSS	Gibco	14025-076
Ficoll-Paue PLUS	GE Healthcare	GE17-1440-03
Golgi Stop	BD biosciences	51-2092KZ
Primocin	Invivogen	ant-pm-05
PMA	Sigma-Aldrich	P1585
Foxp3 staining buffer kit	TONBO Biosciences	TNB-0607-KIT
Strepavidin	Leinco Technologies	S203
Recepie		
cR10: RMPI, 10% Fetal Calf serum, 1 mM sodium pyruvate, 1 mM nonessential amino acids, 10 mM HEPES, 1% L-glutamine, 1% Penicillin/Streptavidin, 50 μM BME		
Wash buffer: RPMI with 2% FCS, pyruvate, 10 mM HEPES, and 1% Penicillin/Streptavidin		
FACS buffer: water, 10x PBS, 0.9% azide, 1% Newborn Calf Serum.		
Permeabilization buffer: water, TONBO Foxp3 staining kit Perm Buffer (10x)		

Table S2.1 PBMC panel

Marker	Tag	Channel	Have expression on which cell
Viability	LIVE DEAD blue	UV6	
CD25	BV421	V1	activated T cells, regulatory T cells and some B cells.
CD45RA	cFluor V450	V3	naïve T cells and some memory T cells
IgM	BV510	V7	class switched memory B cells and naïve B cell
CD3	BV570	V8	T cells and NKT cells
CD56	BV750	V14	NK cells, NKT cells and a small subset of T cells
PD1	BV785	V15	activated T cells, B cells, and myeloid cells
CD8	cFluor B532	B2	cytolytic T cells and NKT cells
CD14	cFluor B548	B3	monocytes and macrophages
HLA-DR	cFluor B690	B9	B cells, monocytes, macrophages and dendritic cells.
CD4	cFluor YG584	YG1	helper T cells, monocytes (low level) and macrophages (low leve
CD16	cFluor BYG610	YG3	NK cells, some macrophages and monocytes
IgD	cFluor BYG667	YG5	naïve B cells
CD11c	cFluor BYG781	YG9	dendritic cells, small subset of monocytes and macrophages
CD127	cFluor R659	R1	T cells and some B cells
CD19	cFluor R685	R3	B cells (not plasma), follicullar DC
CD123	cFluor R720	R4	basophils and plasmacytoid dendritic cells
CD45	cFluor R780	R7	all leukocytes
CD27	cFluor R840	R8	memory B cells and activated T cells

Table S2.2 NK panel

Marker	Tag	Channel	What is this surface marker for
CD3	BUV395	UV2	T cell marker
Live dead blue		UV6	cell viability when staining
CD11b	BUV563	UV9	maturation marker
NKG2D	BUV737	UV14	activation receptor, maturation marker
CD57	Pacific Blue	V3	maturation marker
Ki-67	BV 605	V10	proliferation marker
NKG2A	BB700	B9	inhibitory receptor, maturation marker
NKp44	PE	YG1	activating receptor (do not expressed in resting state)
NKG2C	PE-Vio®770	YG9	activation marker, maturation marker
CD56	APC	R1	NK cell marker
CD69	APC/FireTM	R7	activation marker

Table S3. PBMC subpopulation

	Sample:	B cell | Freq. of live cells	NK cells | Freq. of live cells	T cells | Freq. of live cells	myeloid cells | Freq. of live cells	classic monocyte | Freq. of live cells	non classic monocyte | Freq. of live cells	DC | Freq. of live cells	mDC | Freq. of live cells	pDC | Freq. of live cells
Pt 204	E3 Panel A.fcs	4.40	4.13	70.70	12.30	7.71	0.12	4.17	0.55	0.17
Pt 194.1	E5 Panel B.fcs	9.25	2.32	78.50	5.46	2.74	0.14	2.19	0.87	0.28
AMC 002	E7 Panel C.fcs	6.66	2.76	75.20	9.74	6.30	0.18	3.09	0.98	0.49
Pt 227	E3 Panel A.fcs	3.56	4.79	83.20	4.62	2.88	0.23	1.44	0.56	0.43
Pt 56	E5 Panel B.fcs	5.30	2.15	82.90	4.05	0.98	0.32	2.64	0.17	0.06
MCIA 0362	E7 Panel C.fcs	3.97	7.22	74.30	6.27	3.26	0.59	2.09	0.41	0.46
Pt174	E5 Panel B.fcs	1.01	2.31	81.40	6.79	5.33	0.03	1.36	0.34	0.43
Pt191	E7 Panel C.fcs	1.30	3.71	78.10	7.76	6.09	0.15	1.31	0.59	0.16
MCIA0361	E3 Panel A.fcs	1.40	2.96	84.90	5.46	3.69	0.11	1.55	0.59	0.36
Healthy	low	6.20	2.80	41.00	4.10	1.91	0.10	N/A	0.40	0.10
range	high	20.20	15.50	81.00	26.30	16.40	1.40	N/A	3.80	1.10

	Sample:	TFH | Freq. of live cells	NK cells/CD56bri | Freq. of Parent	NK cells/CD56dim | Freq. of Parent	naive B cell and unswiched memory B cell | Freq. of B cell	class switched memory B cells | Freq. of B cell	IgM- class switched memory B cells | Freq. of B cell	IgM+ class switched memory B cells | Freq. of B cell	naive B cells | Freq. of B cell	unswitched memory B cells | Freq. of B cell
Pt 204	E3 Panel A.fcs	4.27	7.46	81.40	86.10	13.80	7.33	2.21	75.90	9.43
Pt 194.1	E5 Panel B.fcs	2.77	10.80	74.60	93.40	6.51	3.38	0.56	83.00	9.64
AMC 002	E7 Panel C.fcs	1.85	7.22	73.20	91.40	8.31	5.25	0.46	70.40	20.10
Pt 227	E3 Panel A.fcs	2.50	2.13	92.50	81.00	18.70	12.70	1.55	60.30	20.00
Pt 56	E5 Panel B.fcs	3.10	12.70	57.90	93.10	6.61	2.25	0.39	87.40	5.18
MCIA 0362	E7 Panel C.fcs	4.42	13.60	73.70	90.70	9.12	5.50	0.75	81.00	9.12
Pt174	E5 Panel B.fcs	2.75	13.60	68.10	79.40	20.40	13.20	2.32	74.20	4.41
Pt191	E7 Panel C.fcs	2.81	16.50	52.80	91.10	8.86	4.53	0.98	85.40	5.51
MCIA0361	E3 Panel A.fcs	3.96	6.93	76.20	80.50	19.00	12.50	0.35	70.20	8.10
Healthy	low	0.4	1.00	75.00	52.00	2.00	N/A	N/A	N/A	N/A
range	high	1	28.00	99.00	99.00	29.00	N/A	N/A	N/A	N/A

Table S4. Titrated antibody usage

Antigen	Fluorochrome	Volume (ul) for 5e5cells
CD56	BV750	2.5
CD3	BV570	2.5
PD-1	BV785	5
IgM	BV510	5
CD16	PE/Dazzle 594	5
CD56	APC	2.5
CD3	BUV395	1.25
CD19	BV785	2.5

Table S5. Expression of surface marker in NK panel after activated.

Sample\Expression(MFI)	CD69	NKG2A	NKG2D	Ki67	NKp44	NKG2C
Not activated	3004	4873	4016	-61	435	2347
200ng/ml PMA 1h	3668	6461	3454	1402	985	2887
100ng/ml PMA 1h	4195	6349	3318	1444	987	2820
100ng/ml PMA 4h	8053	8017	4338	2403	1784	4255
5000U/ml IL-2 1h	3230	7041	3948	933	600	2887
1000U/ml IL-2 1h	3499	7285	4017	849	550	2744
1000U/ml IL-2 4h	4158	7333	3750	1285	878	3184
100U/ml IL-2 24h	4715	6269	2961	805	1340	2132
Unstained	311	870	475	1152	795	197

The Ki67 and NKp44 is not expressed on resting NK cells. After activated by 100ng/ml PMA for 4h, the Ki67 and NKp44 expression increased. We picked 100ng/ml PMA for 4h for the positive single-color control

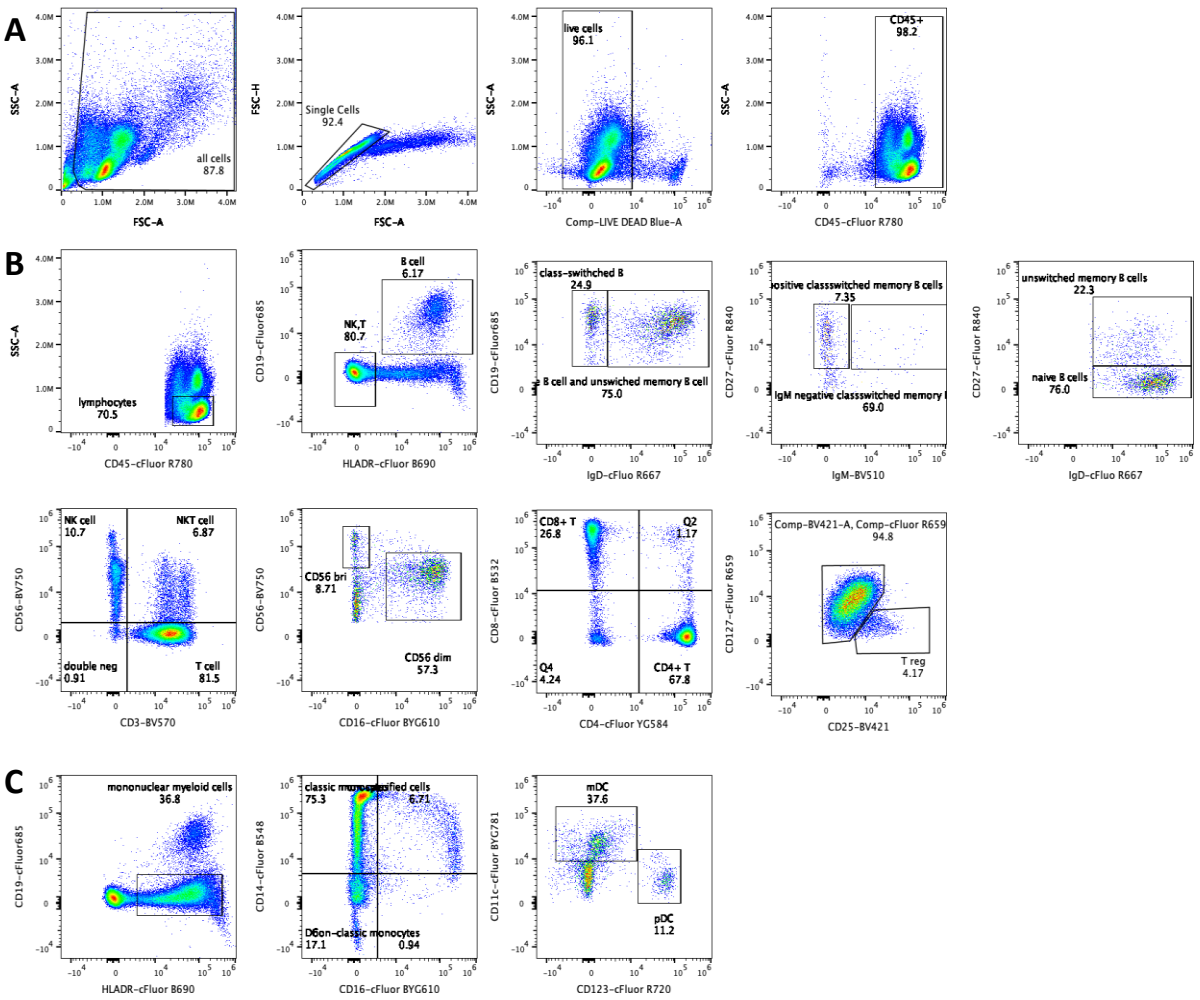

Figure S1 PBMC subpopulation in the 05/17/23 LRS chamber Gating strategy. A. Live leukocytes from all PBMC. Single cell gate exclude all doublets in the larger FSC-SSC gate. Live PBMCs were identified by Live/Dead Blue signals in single cell gate and the immune cells were identified by CD45 positive signals in live cells. B. Lymphocytes from live leukocytes. Lymphocytes were identified by side scatter characteristics in the CD45+ gate. B cells are HLADR+CD 19+ cells in all the lymphocytes, and the double negative population is gated as NK and T cells. The naïve B cells and the unswitched memory B cells are categorized by positive IgD expression in B cell population, and the class-switched memory B cells are categorized by IgD- in the same population. C27 signal is used to distinguish naïve B cells (negative) from the unswitched memory B cells (positive). The class-switched memory B cells are further divided into IgM positive class-switched memory B cells and IgM negative class-switched memory B cells. NK cells are identified by CD3-CD56+ in all the NK and T cells, while T cells are CD3+CD56- and NKT cells are double positive. The NK cells are further divided into two subpopulations based on CD56 and CD16 signals: CD56 bright population (CD56bri CD16-) and CD56 dim population (CD56dim CD16+). T cells are divided into CD4+ T cells, which plays the most important role in regulating and CD8+T cells, which is also know as cytolytic T cells. Treg (regulatory T cells) is characterized by CD35+C127- from CD4+ T cell. C. Monocytes gate from live leukocytes. The mononuclear myeloid cells are categorized by HLADR+CD 19- in all CD45+ cells. They are divided into classic monocytes (CD16-CD14+), nonclassic monocytes (CD16+CD14-) and DC (dendritic cells, CD16-CD14-). mDC (myeloid dendritic cells) is categorized by CD123-CD11c+ and pDC(plasmacytoid dendritic cells) by CD123+CD11c- in DC gate.

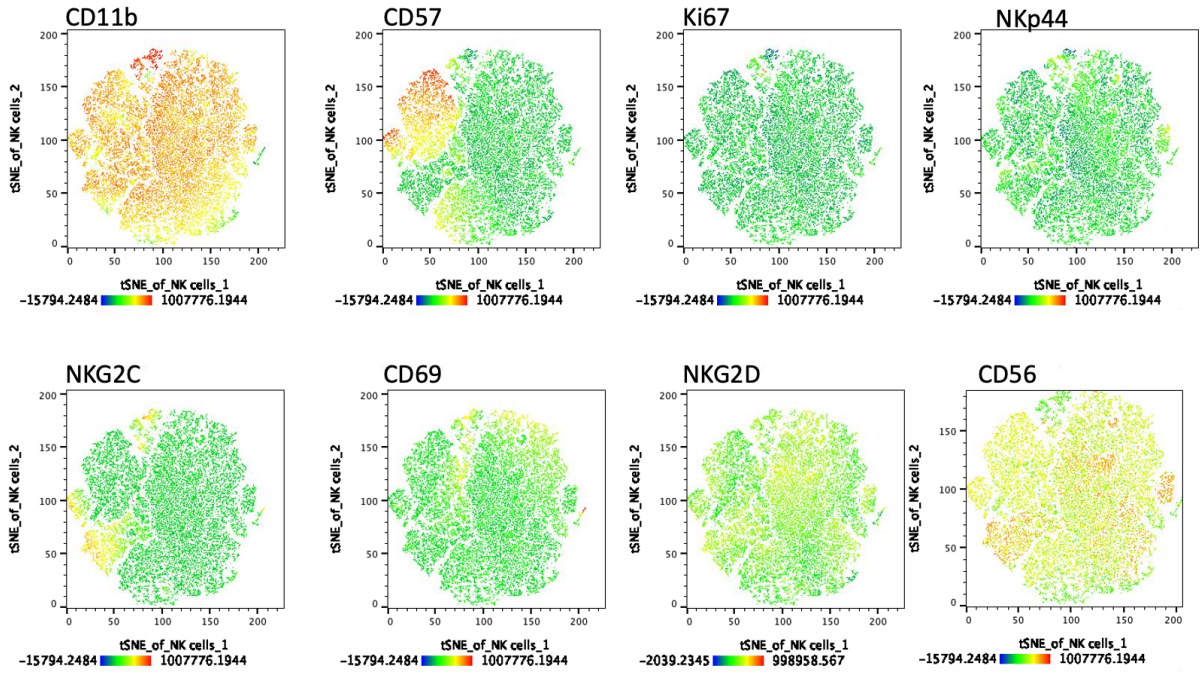

Figure S2 Representative NK panel 2D tSNE map of concatenated samples. The color spectrum represents individual marker-expression levels. Red: high expression; Dark green: no expression.